Author: Lin, Jingwen
Title: Generation of genetically attenuated blood-stage malaria parasites : characterizing growth and virulence in a rodent model of malaria
Issue Date: 2013-09-03

CHAPTER 5

Malaria Parasites Lacking Critical Proteases Involved In Hemoglobin Degradation Are Viable and Are Less Sensitive To Chloroquine

Jing-wen Lin[1], Roberta Spaccapelo[2], Evelin Schwarzer[3], Mohammed Sajid[1], Takeshi Annoura[1], Blandine M.D. Franke-Fayard[1], Séverine Chevalley-Maurel[1], Jai Ramesar[1], Elena Aime[2], Barbara Capuccini[2], Anna M. Mommaas-Kienhuis[4], Paolo Arese[3], Katrien Deroost[5], Tom O'Toole[6], Frans Prins[7], Abraham J. Koster[4], Andrea Crisanti[8], Philippe E. Van den Steen[5], Hans J. Tanke[7], Raimond B. G. Ravelli[4], Chris J. Janse[1] and Shahid M. Khan[1]

[1]Leiden Malaria Research Group, Department of Parasitology, [4]Section Electron Microscopy, Department of Molecular Cell Biology, [7]Department of Pathology, Leiden University Medical Centre, Leiden, The Netherlands
[2]Department of Experimental Medicine, University of Perugia, Piazzale Gambuli , Perugia, Italy
[3]Department of Genetics, Biology, and Biochemistry, University of Torino Medical School, Torino, Italy
[5]Laboratory of Immunobiology, Rega Institute for Medical Research, University of Leuven, Leuven, Belgium
[6]Department of Molecular Cell Biology and Immunology, Vrije University Medical Center, 1007 MB Amsterdam, The Netherlands
[8]Department of Biological Sciences, Imperial College London, South Kensington Campus, SAF, London, SW7 2AZ, UK

Submitted manuscript

Abstract

Survival of *Plasmodium falciparum* parasites inside erythrocytes is considered to depend on hemoglobin digestion. This degradation occurs inside a specialized digestive vacuole (DV) by a number of functionally overlapping and redundant hemoglobinases including the endoproteases (plasmepsins and falcipains) that perform the initial cleavage of hemoglobin. To study *Plasmodium* hemoglobin proteolysis *in vivo*, we used the rodent parasite *P. berghei* that, like the human parasite *P. vivax*, has only one DV plasmepsin and is restricted to reticulocytes. Unexpectedly it was possible to create mutants lacking enzymes known to initiate hemoglobin digestion that can complete development in reticulocytes without hemozoin formation, a detoxification product of hemoglobin degradation. Furthermore, these mutants were more resistant to chloroquine but equally sensitive to artemisinin as compared to wild-type parasites. These observations have important implications for *Plasmodium* drug development and drug resistance, in particular for malaria parasites that preferentially develop inside reticulocytes.

Introduction

Clinical symptoms of malaria are associated with replication of *Plasmodium* parasites inside red blood cells (RBC). Human *P. falciparum* parasites ingest and catabolize more than half of the hemoglobin (Hb) present in the erythrocyte [1,2]. The amino acids derived from Hb proteolysis are used for protein synthesis and energy metabolism and, as malaria parasites have a limited capacity to synthesize amino acids *de novo*, digestion of Hb is believed to be essential for successful parasite replication [1,3,4]. However, human Hb is a poor source of methionine, cysteine, glutamine and glutamate and contains no isoleucine [5-7], and *P. falciparum* blood-stage parasite growth is most effective in culture medium supplemented with these amino acids, especially isoleucine [4-6]. These data indicate that *P. falciparum* parasites not only rely on Hb digestion to acquire amino acids, but also import exogenous amino acids [4,8]. However, growth of *P. falciparum* blood-stages in culture is completely interrupted when Hb proteolysis is blocked by specific inhibitors targeting *Plasmodium* proteases involved in this pathway [1,4]. This proteolysis of Hb is accompanied by the release of free heme, which is highly cytotoxic for the parasite, it is rapidly detoxified by dimerization and then crystallization into a product known as hemozoin (Hz). Therefore, both Hb degradation and heme detoxification are considered to be essential for *P. falciparum* survival [1,9].

The digestion of Hb is a conserved and semi-ordered process, which principally occurs within the acidic digestive vacuole (DV). The important initial cleavage of native Hb is mediated by aspartic and papain-like cysteine endoproteases. In the *P. falciparum* DV there are four aspartic proteases termed plasmepsins and two papain-like cysteine proteases termed falcipains capable of hydrolyzing host Hb [10-14]. After the first cleavage, Hb unfolds and becomes susceptible for further proteolysis by downstream proteases. Gene disruption studies of hemoglobinases demonstrate that *P. falciparum* has developed redundant and overlapping enzymatic systems for Hb degradation. Specifically, the multiple *P. falciparum* plasmepsins and falcipains overlap in function and there is extensive functional redundancy within and between these 2 families [4,15-17]. Most studies on hemoglobinases have been performed using *P. falciparum* blood-stages cultured *in vitro* and it remains to be proven that observations derived from loss-of-function assays in culture can also be directly translated to parasites replicating *in vivo*. Further, *P. falciparum* infects mature RBC and it is unknown whether the observations on Hb digestion made with *P. falciparum* in mature RBC also apply to *P. falciparum* and other *Plasmodium* species that can invade and develop inside young RBC, reticulocytes.

Here we studied the functional redundancy amongst the enzymes involved in Hb digestion both *in vivo* and *in vitro*, using the rodent malaria parasite *P. berghei* that, like the human

malaria parasite *P. vivax*, preferentially invades reticulocytes. Using a reverse genetics (loss-of-function) approach we demonstrate that 6 out of 8 genes predicted to encode *P. berghei* hemoglobinases are dispensable, demonstrating a high level of functional redundancy of these enzymes *in vivo*. Surprisingly, we were able to generate a *P. berghei* double gene deletion mutant lacking both plasmepsin-4 (PM4), the syntenic ortholog of all four *P. falciparum* plasmepsins I-IV [18], and berghepain 2 (BP2), the syntenic ortholog of the DV falcipains (falcipain 2 and 3), i.e. the enzymes involved in the initial and critical cleavage of host Hb. These mutants were able to mature into schizonts inside reticulocytes without producing Hz. Furthermore, these parasites are less sensitive to the action of chloroquine, a drug that principally acts by inhibiting Hz formation, but retain sensitivity to artemisinin. Our observations thus demonstrate that malaria parasites can multiply in reticulocytes without producing Hz, which show increased resistance to antimalarials that target heme detoxification. Currently, targeting *Plasmodium* enzymes that interfere with heme detoxification mechanisms is a major focus of drug development (www.mmv.org) and our observations not only have important implications for development of novel antimalarials but also suggest alternative mechanisms of drug-resistance. This is especially true for parasites with a preference for reticulocytes, such as the important human parasite *P. vivax*, for which evidence exists that chloroquine resistance is different from that described in *P. falciparum* [19,20]. In addition, mutant parasites that produce little or no Hz are excellent tools to analyze both the mode of action of drugs targeting Hz formation and to examine the possible pathological role of Hz during infections *in vivo*.

Results

High degree of functional redundancy amongst *Plasmodium* hemoglobinases

In order to gain an understanding on the essential nature of individual enzymes involved in *P. berghei* Hb digestion, we performed a systematic loss-of-function analysis on 8 predicted hemoglobinases that are orthologs of *P. falciparum* proteases with a role in Hb digestion and/or located in the DV. These enzymes (Table 1) are: the aspartic protease PM4 which is the single syntenic ortholog of the four plasmepsins in *P. falciparum* (plasmepsin I-IV) [18]; the papain-like cysteine protease BP2, which is the single syntenic ortholog of the *P. falciparum* DV falcipains 2 and 3 [21]; the M16 metalloprotease *berghei*lysin (BLN), the ortholog of *P. falciparum* falcilysin [22]; the dipetidyl peptidase DPAP1 or cathepsin C [23]; and four aminopeptidases, i.e. aminopeptidase P (APP) [24,25], M1-family alanyl aminopeptidase (AAP, ortholog of *P. falciparum* M1AAP) [25,26], M17-family leucyl

aminopeptidase (LAP, ortholog of *P. falciparum* M17LAP) [25,27] and M18-family aspartyl aminopeptidase (DAP, ortholog of *P. falciparum* M18DAP) [25]. In addition, we performed gene loss-of-function analyses for the heme detoxification protein (HDP), which is involved in the conversion of heme into Hz [28], as well as for three enzymes that are related to some proteases of the DV, but that do not have a proven role in Hb digestion and of which the cellular location is unknown. These enzymes are berghepain 1 (BP1, the ortholog of *P. falciparum* falcipain 1, FP1) [29-31] and 2 dipetidyl peptidases, DPAP2 and DPAP3 [32].

Table 1. Genes targeted in this study

Product name *P. falciparum* **Gene ID**	**Localization (Pf)**	**Essential for blood stages (Pf)**	**product name** *P. berghei* **Gene ID**	**Essential for blood stages (Pb)** *
aspartic endoprotease				
plasmepsin I (PM I) PF3D7_1407900	DV [13]	no [16,17,33,34]	-	-
plasmepsin II (PM II) PF3D7_1408000	DV [13,35]	no [16,17,33,34]	-	-
plasmepsin IV (PM IV) PF3D7_1407800	DV [13]	no [16,17,33,34]	plasmepsin 4 (PM4) PBANKA_103440	no, [18]
plasmepsin III (PM III) PF3D7_1408100	DV [13]	no [16,17,33,34]	-	-
papain-like cysteine endoprotease				
falcipain 2a (FP 2a) PF3D7_1115700	DV [36-38]	no [15,29]	berghepain-2 (BP2) PBANKA_093240	no
falcipain 2b (FP 2b) PF3D7_1115300	DV [38]	no [29]	-	-
falcipain 3 (FP 3) PF3D7_1115400	DV [36,38]	yes [29]	-	-
metallopeptidase				
falcilysin (FLN) PF3D7_1360800	DV, MT, AP [22]	yes [22]	*berghei*lysin (BLN) PBANKA_113700	yes
dipeptidyl aminopeptidase				
dipeptidyl aminopeptidase 1 (DPAP1) PF3D7_1116700	DV [23]	yes [23]	dipeptidyl aminopeptidase 1 (DPAP1) PBANKA_093130	no
aminopeptidases				
aminopeptidase P (APP) PF3D7_1454400	DV, CY [24,25]	yes [24,25]	aminopeptidase P (APP) PBANKA_131810	no
M1- family alanyl aminopeptidase (M1AAP) PF3D7_1311800	DV, NU [25,26]	yes [25]	M1- family alanyl aminopeptidase (AAP) PBANKA_141030	yes
M17-family leucyl aminopeptidase (M17LAP) PF3D7_1446200	DV [39], CY [25,27]	yes [25]	M17-family leucyl aminopeptidase (LAP) PBANKA_130990	no
M18-family aspartyl aminopeptidase (M18DAP) PF3D7_0932300	CY [25]	no [25]	M18-family aspartyl aminopeptidase (DAP) PBANKA_083310	no

heme detoxification protein				
heme detoxification protein (HDP) PF3D7_1446800	DV [28]	yes [28]	heme detoxification protein (HDP) PBANKA_131060	yes
papain-like cysteine proteases				
falcipain 1 (FP1) PF3D7_1458000	Apical end of merozoites [31]	no [29,30]	berghepain 1 (BP1) PBANKA_132170	no
dipeptidyl aminopeptidases				
dipeptidyl aminopeptidase 2 (DPAP2) PF3D7_1247800	-	-	dipeptidyl aminopeptidase 2 (DPAP2) PBANKA_146070	no
dipeptidyl aminopeptidase 3 (DPAP3) PF3D7_0404700	-	yes [32]	dipeptidyl aminopeptidase 3 (DPAP3) PBANKA_100240	no

DV: digestive vacuole; MT: mitochondrion; AP, apicoplast; CY, cytosol; NU, nucleus
*, the phenotype observed in this study.
-, no published data.

We used standard genetic modification technologies to delete the genes encoding above mentioned enzymes and successfully generated gene deletion mutants for *pm4*, *bp1*, *bp2*, *dpap1*, *dpap2*, *dpap3*, *app*, *lap* and *dap* (Figure S1–3), whereas multiple attempts to disrupt *bln*, *aap* and *hdp* were unsuccessful (Table S1). The successful selection of gene-deletion mutants for 6 out of 8 predicted hemoglobinases indicates a high level of redundancy amongst the *P. berghei* proteases involved in Hb digestion. We previously reported that disruption of *pm4* results in the lack of all aspartic protease activity in the DV [18]. Also in *P. falciparum* it has been shown that blood stages are able to survive without DV aspartic protease activity [16]. We were able to select mutants that lack genes encoding DPAP1, APP and LAP, which is unexpected since the *P. falciparum* orthologs of these genes have been reported to be refractory to targeted gene disruption (Table 1; [23,25]. We were unable to select parasites lacking expression of AAP, HDP and BLN and in *P. falciparum*, the orthologous genes of *aap*, *hdp* and *bln* have also been reported to be resistant to disruption [22,25,28].

Mutants lacking expression of PM4, DPAP1, BP1, LAP or APP exhibit a significant reduction in growth and of these Δ*pm4* and Δ*app* also produce less hemozoin

We determined the *in vivo* asexual multiplication rate, i.e. growth rate, for all nine gene-deletion mutants (Table 2). We previously reported that the growth rate of Δ*pm4* parasites was moderately but significantly reduced compared to wt parasites, with multiplication rates ranging from 5.8 to 7.7-fold per 24 hours compared to a consistent 10-fold in wt parasites [18]. These multiplication rates were calculated during the initial

phase of infection after mice had been infected with a single parasite. Parasites lacking the DV dipeptidyl aminopeptidase DPAP1 (Δ*dpap1*) and BP1 (Δ*bp1*) have a comparable reduction in growth with multiplication rates of 7.7 and 6.8, respectively, and growth rates of Δ*lap* and Δ*app* were much more reduced with multiplication rates of only 3.3 and 4.6, respectively (Table 2). The Δ*bp2* and Δ*dap* mutants had normal, wt-like growth rates and growth rates of Δ*dpap2* and Δ*dpap3* mutants were only slightly (but not significantly) reduced (Table 2).

Table 2. Blood-stage growth and virulence characteristics of gene-deletion mutants

Gene deletion mutant	Day to 0.5-2% parasitemia [1]	multiplication rate [2]	Hz production[3]
wt [4]	8 (0.2), n=40	10.0 (0.7)	198.8 (69.8)
Δ*pm4*-a [5]	9-11, n>10	5.8(0.5)-7.0 (1.0) ***	129.5 (41.7) ***
Δ*pm4*-b	9 (0), n=2	7.7 (0) ***	134.5 (47.6) ***
Δ*bp2*-a	8 (0), n=5	10.0 (0)	177.5 (45.1)
Δ*bp2*-b	8 (0), n=6	10.0 (0)	188.4 (71.5)
Δ*dpap1*-a	9.5 (0.7), n=2	7.0 (1.0) ***	174.6 (34.0)
Δ*dpap1*-b	9 (0), n=4	7.7 (0) ***	189.2 (62.7)
Δ*app*-a	12 (0), n=1	4.6 (0) ***	131.8 (50.5) ***
Δ*app*-b	12 (0), n=4	4.6 (0) ***	111.4 (49.7) ***
Δ*dap*	8 (0), n=3	10.0 (0)	223.8 (65.7)
Δ*lap*	15.5 (0.7), n=2	3.3 (0.2) ***	213.6 (78.7)
Δ*bp1*-a	9.7 (0.6), n=3	6.8 (0.8) ***	186.2 (49.2)
Δ*bp1*-b	9 (0), n=1	7.7 (0) ***	n.d
Δ*dpap2*	8.3 (0.4), n=4	9.4 (1.0)	187.8 (64.6)
Δ*dpap3*-a	8.3 (0.6), n=3	9.2 (1.3)	184.5 (86.3)
Δ*dpap3*-b	8 (0), n=5	10.0 (0)	193.3 (46.8)
Δ*pm4*Δ*bp2*-a	12, 16, 20, n=3	3.4 (1.1) ***	27.2 (36.5) ***
Δ*pm4*Δ*bp2*-b	21, 24, n=2	2.3 (0.1) ***	46.1 (51.2) ***

n.d., not determined

[1] The day on which the parasitemia reach 0.5–2% in mice infected with a single parasite during cloning assays. The mean of one cloning experiment and standard deviation were shown. n, the number of mice tested. For the Δ*pm4*Δ*bp2* mutants, due to large variation, the days of which individual clone were shown.

[2] The multiplication rate of asexual blood stages per 24 hours is determined as following: when one clone in infected mice takes 8 days to parasitemia reach 0.5–2%, the multiplication rate is determined as 10. Mean values and standard deviations of each line were shown, student T-test, ***, P<0.0001.

[3] Hz production values were determined by relative light intensity of Hz crystals in individual schizont under polarized light microscopy (Figure 1). Mean values and standard deviations were shown, student T-test, ***, P<0.0001.

[4] wt, wild type *P. berghei* ANKA lines, including cl15cy1, 676m1cl1, 1037m1f1cl1, the data were collected more than 10 independent experiments.

[5] *pm4* gene deletion mutants generated in Spaccapelo,R. *et al*, 2010 (ref [18])

We next determined the amount of Hz generated in schizonts of all mutants as a measure of Hb digestion. The total amount of Hz was quantified in individual schizonts by measuring relative light intensity (RLI) in schizonts using reflection contrast polarized light microscopy [33,34]. Only schizonts containing 8–24 nuclei were selected, thereby

selecting those parasites that were fully mature and in the process of mitosis (Figure 1A).

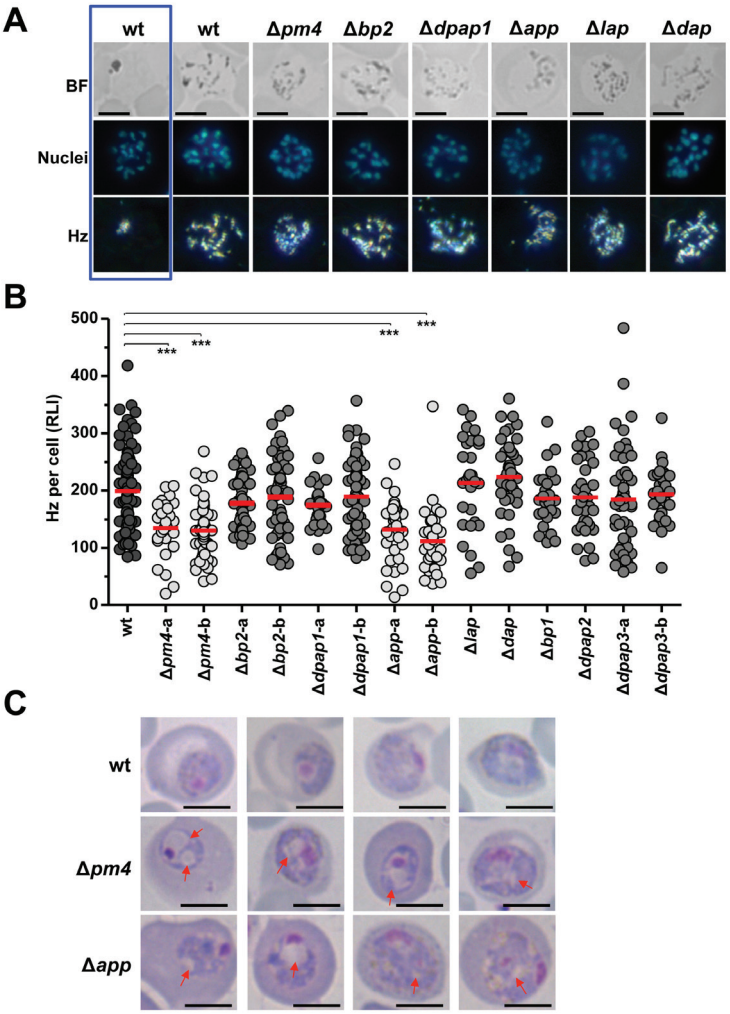

Figure 1. Hemozoin levels in parasite mutants lacking expression of enzymes involved in hemoglobin digestion

A. Hemozoin (Hz) crystals in schizonts as observed by light and reflection contrast polarized microscopy. Maturing schizonts were selected with scattered Hz that was not yet clustered into the characteristic single cluster that is observed only in fully segmented schizonts (boxed). Representative schizonts of wild-type (wt) and 6 mutants (Δ*pm4*, Δ*bp2*, Δ*dpap1*, Δ*app*, Δ*lap* and Δ*dap*) are shown. BF, bright-field; Nuclei, nuclei stained with Hoechst-33342.

B. The amount of Hz in individual schizonts (n>30/group) determined by measuring relative light intensity (RLI) of polarized light. The Hz level in mutants lacking expression of plasmepsin4 (Δ*pm4*) and aminopeptidase P (Δ*app*) is significantly different from wt-schizonts (student T-test; *** P<0.0001).

C. Aberrant morphology of Δ*pm4* and Δ*app* trophozoites exhibiting reduced Hz production and showing an accumulation of translucent vesicles (indicated by arrows) in their cytoplasm. Scale bars, 5 µm.

Compared to wt schizonts, only Δ*pm4* and Δ*app* mutants showed a clear and significant reduction in Hz production, whereas all the other 7 mutants produced similar levels of Hz compared to the wt parasite (Figure 1A&B, Table 2). The Hz reduction in Δ*app* mutants is unexpected since APP was shown to be involved in generating free amino acids from small peptides liberated from successive steps of hemoglobin digestion after heme is released from the initial cleavage of Hb. Trophozoites of Δ*app* and Δ*pm4* mutants have an aberrant morphology as visible on Giemsa stained blood smears, exhibiting an accumulation of translucent vesicles inside their cytoplasm (Figure 1C). These observations indicate that a number of gene-deletion mutants for *P. berghei* hemoglobinases have reduced parasite multiplication rates, but only Δ*pm4* and Δ*app* mutants are impaired in Hz production.

Blood-stage mutant parasites lacking both PM4 and BP2 are viable but have a reduced rate of growth

We examined whether we could generate *P. berghei* parasites in which the genes encoding both PM4 and BP2 (Δ*pm4*Δ*bp2*) are deleted. The simultaneous absence of these two enzyme activities in *P. berghei* is expected to result in the absence of Hb hydrolysis in the DV, since in *P. berghei* PM4 is the only vacuolar aspartic protease, and BP2 is the single syntenic ortholog of the two cysteine endoproteases found in the DV of *P. falciparum* (falcipain 2 and 3). Unexpectedly, we were able to generate double gene-deletion mutants that lack expression of both PM4 and BP2 (Figure S4). Blood-stages of Δ*pm4*Δ*bp2* have a strongly reduced growth rate in cloning assays with multiplication rates ranging from 2.2 to 4.6, which is significantly lower than wt ($P< 0.0001$) and Δ*pm4* parasites ($P<0.0001$) (Table 2). In long-term infections in BALB/c and C57BL/6 mice, there is an initial slow rise in Δ*pm4*Δ*bp2* parasite numbers. However, parasitemia can reach high levels (up to 50%) when these mice start to produce reticulocytes in response to the infection (Figure S5). In the infections with high parasitemias, mature schizonts were present in the peripheral blood circulation, most of which contained 8–12 merozoites (Figure S2A). Furthermore, in contrast to wt-infected mice (but similar to Δ*pm4*-infected mice) C57BL/6 mice infected with Δ*pm4*Δ*bp2* did not develop symptoms of experimental cerebral malaria (ECM). In contrast to Δ*pm4* infections which can only be resolved by BALB/c mice [18], both C57BL/6 and BALB/c mice were able to resolve a Δ*pm4*Δ*bp2* infection, resulting in undetectable parasitemias by microscopic analysis 3–6 weeks after infection (Figure S5).

Schizonts of Δ*pm4*Δ*bp2* are smaller in size and produce fewer merozoites than wt-schizonts

Although wt *P. berghei* parasites preferentially invade reticulocytes, merozoites can also invade and develop in mature RBC producing mature schizonts both *in vivo* and *in vitro* [35]. Even though ring forms of Δ*pm4*Δ*bp2* were observed in both mature RBC and reticulocytes, schizonts were exclusively found in reticulocytes as observed on Giemsa-stained slides (data not shown). This indicates that Δ*pm4*Δ*bp2* parasites, while retaining their ability to invade mature RBC, are unable to develop into fully segmented schizonts in mature erythrocytes. Light microscopy examination of Giemsa-stained blood-stages showed that mature Δ*pm4*Δ*bp2*-schizonts were small and left a large volume of the infected RBC (iRBC) unoccupied (occupying only 25–65%), whereas wt-schizonts occupied 60–90% of the host iRBC (Figure 2A). We also examined the sizes of live wt- and Δ*pm4*Δ*bp2*-schizonts by imagestream flow cytometry. Both wt- and Δ*pm4*Δ*bp2*-parasites express GFP under the control of the schizont/merozoite-specific *ama-1* promoter, therefore iRBCs with mature schizonts were selected based on their GFP and Hoechst fluorescence (Figure 2B). Analysis of the size of iRBCs and schizonts of Δ*pm4*Δ*bp2* and wt parasites demonstrated that Δ*pm4*Δ*bp2*-schizonts were significantly smaller than wt schizonts (P<0.0001; Figure 2B). In addition, Giemsa-stained parasite analysis indicated that Δ*pm4*Δ*bp2*-schizonts had fewer merozoites than wt-schizonts (Figure 2A). We therefore quantified the total DNA content of mature Δ*pm4*Δ*bp2*-schizonts by measuring Hoechst fluorescence intensity using both standard and imagestream flow cytometry. Both methods demonstrated that mature Δ*pm4*Δ*bp2*-schizonts have significantly less total DNA compared to wt-schizonts (55–60% of wt, P<0.0001), indicating a significant reduction in the total number of merozoites per individual schizonts (Figure 2C). The reduction in the number of daughter merozoites was also reflected in the intensity of (*ama1* based) GFP expression levels in mature schizonts. In comparison to wt-schizonts, Δ*pm4*Δ*bp2*-schizonts have a 40% reduction in GFP-intensity (P<0.0001), which corresponds to the reduction in total DNA and therefore the number of merozoites per schizont (Figure 2C). Thus, parasites lacking both PM4 and BP2 develop into smaller schizonts and produce less daughter cells compared to wt-schizonts.

The Δ*pm4*Δ*bp2* mutant can develop into mature schizonts in the absence of detectable hemozoin

Many trophozoites of Δ*pm4*Δ*bp2*, as observed by standard light microscopy, have an 'amoeboid-like' appearance, with many translucent vesicles inside the cytoplasm, similar to what we had observed for Δ*pm4* and Δ*app* mutants. Moreover, both Δ*pm4*Δ*bp2*

trophozoites and schizonts have strongly reduced or even no visible Hz (Figure 2 and Figure S5). To analyze these features in more detail we both quantified Hz levels in schizonts and analyzed the ultrastructure of Δ*pm4*Δ*bp2* trophozoites. First, we determined the total

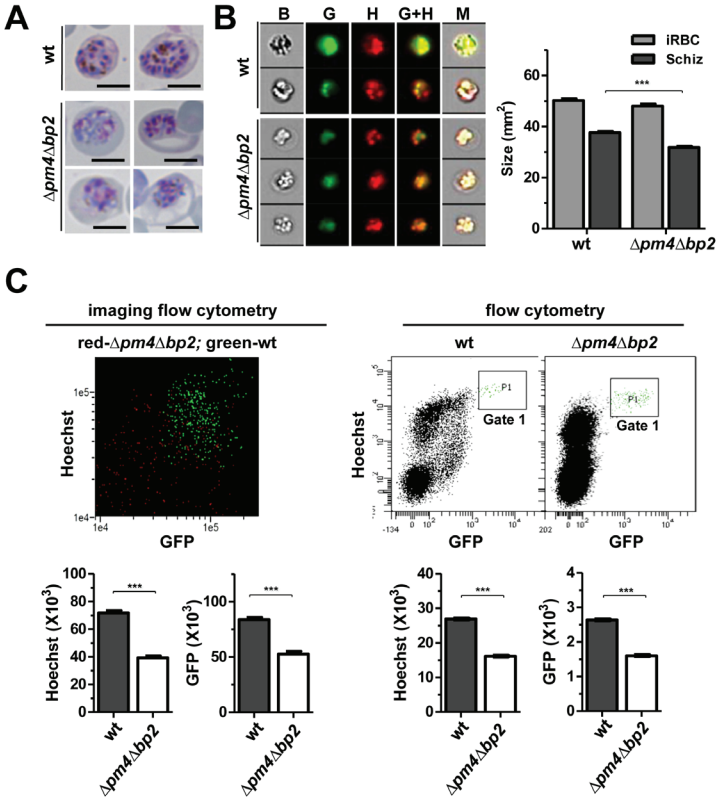

Figure 2. Schizonts of mutants lacking expression of PM4 and BP2 are smaller in size and have fewer merozoites

A. Giemsa-stained schizonts of wt and Δ*pm4*Δ*bp2*–parasites. The Δ*pm4*Δ*bp2* schizonts leave a large volume of the infected RBC unoccupied compared to wt schizonts. Scale Bar, 5 µm.

B. Images of mature schizonts and size measurement (n>250) by imagestream flow cytometry (left and right panels). Both wt- and Δ*pm4*Δ*bp2*-parasites express GFP under the control of the schizont/merozoite-specific *ama-1* promoter and their nuclei were stained with Hoechst-33342. Mature schizonts were selected on the basis of their GFP (G, green) and Hoechst (H, red) fluorescence intensity. The size of iRBCs containing schizonts was measured from the bright-field image (B) and the size of the schizonts was measured from the combined GFP and Hoechst images (G+H) (student T-test, *** P<0.0001). M; all images merged.

C. Determination of the DNA content (Hoechst fluorescence intensity) and the GFP expression in wt and Δ*pm4*Δ*bp2*-schizonts by imaging flow cytometry (left panel) and standard flow cytometry (right panel). Mature schizonts were selected based on their GFP- and Hoechst-fluorescence intensity. The dot plot (upper, left) shows the GFP- and Hoechst fluorescence intensity for individual schizonts in image stream flow cytometry. In standard flow cytometry (upper, right) schizonts were selected for measurement in Gate 1. Schizonts of Δ*pm4*Δ*bp2* contained significantly less DNA and displayed reduced GFP expression (*** P<0.0001, student T-test).

amount of Hz in individual schizonts using reflection contrast polarized light microscopy. Compared to wt-parasites the amount of Hz in schizonts of two independently derived Δ*pm4*Δ*bp2* lines was strongly reduced (13–22% of the wt values, p<0.0001; Figure 3A, Table 2). By polarized light microscopy we found that a large percentage (35–48%) of the Δ*pm4*Δ*bp2*-schizonts were completely Hz-negative, whereas all wt-schizonts were Hz-positive (Figure 3A). The Hz-negative Δ*pm4*Δ*bp2*-schizonts had relative light intensity (RLI) values similar to uninfected RBC. The presence of Hz-negative schizonts indicates that parasites can grow and multiply without Hb digestion. The strong reduction in Hz production per schizont was reflected in reduced Hz deposition in organs of Δ*pm4*Δ*bp2*-infected mice compared to wt-infected mice. In wt-infected mice almost 95% of the Hz produced is deposited in the spleen and liver [36]. We compared Hz-levels in spleen, lungs and liver at different time points in mice infected with wt, Δ*pm4* or Δ*pm4*Δ*bp2* parasites (Figure 3B). Mice infected with Δ*pm4* and Δ*pm4*Δ*bp2* had significantly less Hz deposited in all organs examined compared to wt-infected mice at a comparable parasitemia (56% less, P<0.001; and 87% less, P<0.0001, respectively). In addition, organs of Δ*pm4*Δ*bp2*-infected mice had significantly less Hz than Δ*pm4*-infected mice (72% less; P<0.001) (Figure 3B). The relative differences in Hz deposition in organs of mice infected with the different parasite lines corresponds well with the differences in Hz levels found in schizonts of wt, Δ*pm4* and Δ*pm4*Δ*bp2* parasites, as determined by polarized light microscopy (Figure 3A&B, Table 2). We also confirmed the reduction in Hz production in Δ*pm4*Δ*bp2* trophozoites by quantifying the number of Hz crystals using electron microscopy (Figure 3C). The ultrastructural analysis showed that Δ*pm4*Δ*bp2* trophozoites contained a higher number of cytostome or endocytic vesicles in comparison to wt trophozoites, which were filled with material that was structurally identical to erythrocyte cytoplasm (Figure 3C). Furthermore, in the cytoplasm of 37% of Δ*pm4*Δ*bp2*-trophozoites we observed dark stained (electron dense) vesicles, which were completely absent in wt-parasites (Figure 3C and S6). The presence of increased numbers of these vesicles in the cytoplasm may explain the translucent vesicles observed in trophozoites on Giemsa-stained blood films (Figure S5).

Gametocytes of Δ*pm4*Δ*bp2* are fertile despite their smaller size and reduced hemozoin production

In mice infected with Δ*pm4*Δ*bp2*-parasites, uninuclear parasites with the characteristics of male and female gametocytes were readily detected (Figure S7). However, they were significantly smaller than wt-gametocytes (23% smaller, Figure S7), and their cytoplasm also have strongly reduced or no Hz crystals. Most Δ*pm4*Δ*bp2* male gametocytes produced motile gametes (79.3%±4.6) and conversion rates of Δ*pm4*Δ*bp2* female gametes into

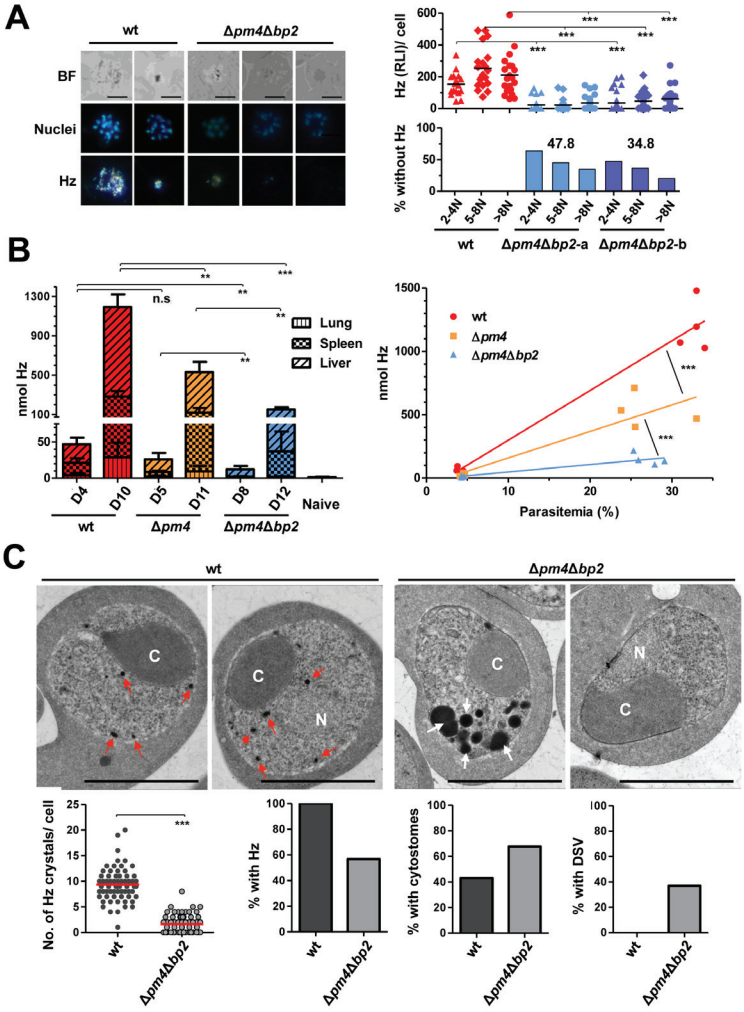

Figure 3. Δ*pm4*Δ*bp2* mutant parasites can develop into mature schizonts with little or no detectable hemozoin

A. The amount of Hz in individual schizonts as determined by measuring relative light intensity (RLI) using reflection contrast polarized light-microscopy. Left panel: Hz crystals in schizonts as observed under polarized light. In Δ*pm4*Δ*bp2* parasites Hz levels are either strongly reduced or absent. Right panel: Hz levels (RLI) in schizonts with 2–4, 5–8 or more than 8 nuclei (N) (n>20 per category). The Hz level in two Δ*pm4*Δ*bp2*-mutants is significantly less than in wt-schizonts across all categories (student T-test, *** P<0.0005). Lower panel: a large proportion of Δ*pm4*Δ*bp2*-schizonts have no detectable Hz crystals under polarized light with RLI levels similar to uninfected RBC. BF, bright field; Nuclei, nuclei stained with Hoechst-33342.

B. Hz levels in different organs of BALB/c mice infected with wt, Δ*pm4* or Δ*pm4*Δ*bp2*-parasites at different days (D) after infection (left panel) and total Hz levels in function of peripheral parasitemia in infected mice (right panel). Not significant (ns), ** p<0.05, *** p<0.0005 (student T-test). **C.** Quantification of Hz crystals, cytostomes (C) and dark-staining vesicles (DSV) in Δ*pm4*Δ*bp2*-and wt-trophozoites. Upper panel: Electron micrographs of representative trophozoites of wt- and Δ*pm4*Δ*bp2*-parasites. Red arrowheads denote pigment crystals (Hz) and white arrow indicate DSVs and light staining nuclei (N). Scale bars, 5 µm. Lower panel: quantification of Hz

crystals (student T-test, *** P<0.0005), cytostomes and DSVs in randomly selected trophozoites (n>50) from electron micrographs (see also Figure S6).

ookinetes were comparable to those of wt-parasites (60.0%±6.1; Figure S7). Analysis of Hz crystals in wt and Δ*pm4*Δ*bp2* ookinetes revealed that these ookinetes had strongly reduced levels of Hz (57% reduction; Figure S7). These observations demonstrate that both asexual and sexual blood-stages can complete development in the absence of PM4 and BP2 to initiate Hb digestion.

The Δ*pm4*Δ*bp2* parasites are more resistant to chloroquine but retain their sensitivity to artemisinin

We tested the sensitivity of the Δ*pm4*Δ*bp2*-parasites to two antimalarial drugs known to interfere with Hb digestion and/or Hz formation, i.e. chloroquine (CQ) and artesunate (AS), an artemisinin derivative via different mechanisms [37,38]. As a control, we used sulfadiazine (SD), an inhibitor of folic acid synthesis with no known role in inhibiting Hb digestion [39]. BALB/c mice infected with either wt- or Δ*pm4*Δ*bp2*-parasites were treated with these drugs when peripheral parasitemia was between 2 and 5%, i.e. at day 6 after infecting mice with 10^4 wt-parasites or at day 9 after infecting mice with 10^5 Δ*pm4*Δ*bp2*-parasites. Treatment with SD as well as AS resulted in a rapid decrease in parasitemia with parasites being undetectable in peripheral blood 3–4 days after AS treatment and 4–5 days after SD treatment, and the profile of drug action being identical for both wt- and Δ*pm4*Δ*bp2*-parasites (Figure 4C). In contrast, whereas wt-infected mice rapidly cleared their infection after CQ treatment with no parasites detectable in peripheral blood 3–4 days after the start of treatment, Δ*pm4*Δ*bp2* infected mice maintained an increasing parasitemia for the first three days of treatment (Figure 4C). After this period, parasitemia started to decline but Δ*pm4*Δ*bp2*-parasites with morphology similar to that of untreated parasites could still be observed by light microscopy (Figure S8A) up to 6 days after initiation of CQ treatment (Figure 4C). The parasitemia in CQ treated mice dropped to submicroscopic level after 7 days of CQ treatment (i.e. day 16 post infection). Interestingly, in untreated mice the Δ*pm4*Δ*bp2* parasitemia similarly dropped around day 15–18 post-infection (Figure S8B), presumably due to an acquired immune response.

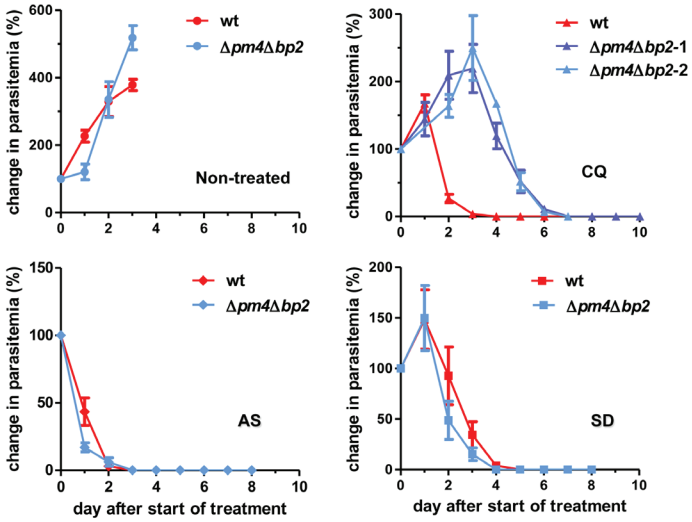

Figure 4. Δ*pm4Δbp2*-schizonts are less sensitive to chloroquine than wt-parasites

Change in parasitemia of mice (n=5) infected with wt- or Δ*pm4Δbp2*-parasites after treatment with chloroquine (CQ; 2 experiments), artesunate (AS) or sulfadiazine (SD). Δ*pm4Δbp2* parasites are less sensitive to CQ but retain the same sensitivity to AS and SD as wt parasites.

Discussion

P. falciparum growth in RBC is considered to be dependent on Hb digestion [40]. In addition to providing amino acids for growth it has been proposed that parasites digest Hb to maintain the intracellular osmolarity of the infected RBC, thereby preventing premature erythrocyte lysis [41], or to make space within the RBC as the parasite expands [42,43]. Our studies, however, provide evidence that *Plasmodium* blood stage parasites, both asexual and sexual forms, can fully mature with little or no Hz production when parasites invade and develop inside reticulocytes indicating that blood stages can growth without or with strongly reduced Hb digestion.

As has been previously reported in *P. falciparum*, we found that a large number of *P. berghei* enzymes predicted to have a role in Hb proteolysis are functionally redundant. The viability of mutant parasites lacking hemoglobinases, indicates either that other enzymes can replace their function(s) or that *P. berghei* can obtain all amino acids from other sources, for example from the catabolism of proteins other than Hb or by scavenging free amino acids from the reticulocyte cytoplasm or serum. On the other

hand, the strong reduction in growth of Δ*pm4*Δ*bp2*-parasites lacking both PM4 and BP2 enzymes, whose *P. falciparum* orthologs are responsible for the initial cleavage of Hb, suggests that Hb is an important amino acid source. The reduced growth rate might, however, also be attributed to the other features associated with reduced Hb digestion, such as limited space inside the RBC for growth resulting in smaller schizonts with fewer merozoites or the loss of parasites that invade mature RBC but are unable to fully mature.

We did not observe replicating Δ*pm4*Δ*bp2*-parasites in mature RBC and in Δ*pm4*Δ*bp2* infections, parasite numbers increased rapidly only when mice start to produce large numbers of reticulocytes, at which stage they can achieve parasitemias as high as 50%. Further, when Δ*pm4*Δ*bp2* ring forms were transferred to culture less than 5% produced mature schizonts, in comparison more than 90% of wt ring forms can develop into fully mature schizonts (data not shown). This is most probably due to the accelerated maturation of reticulocytes in culture [44], which restricts the development of Δ*pm4*Δ*bp2* schizonts. The ability of Δ*pm4*Δ*bp2*-parasites to form merozoites only in reticulocytes is likely related to the greater abundance of amino acids and proteins other than Hb in the reticulocyte compared to mature RBC. Reticulocytes are known to accumulate amino acids for incorporation into Hb [45] and these may be available for direct utilization when the parasite ingests reticulocyte cytoplasm. The Δ*pm4*Δ*bp2*-trophozoites show an increased number of cytostome-vesicles containing RBC cytoplasm, indicating that the absence of PM4 and BP2 does not affect Hb uptake. In addition to cytostomes, we found electron-dense dark-staining vesicles in a large proportion of Δ*pm4*Δ*bp2* trophozoites. Interestingly, very similar vesicles have been observed in *P. falciparum* trophozoites when Hb digestion or Hb trafficking (cytostome formation) have been blocked by inhibitors [46,47]. It has been proposed that these vesicles are derived from the cytostomes and contain concentrated undigested or denatured Hb [47]. In addition to the increased numbers of vesicles in trophozoites, we found that mature Δ*pm4*Δ*bp2*-schizonts and gametocytes have strongly reduced amounts or even no Hz in their cytoplasm, indicating that Hb digestion is strongly impaired. The presence of low Hz amounts in a proportion of Δ*pm4*Δ*bp2*-parasites indicates that some heme is released from Hb in the absence of PM4 and BP2. However, whether this is mediated by a specific, but inefficient, compensatory enzymatic process or is the result of unspecific hemoglobin denaturation is unknown. In *P. berghei* PM4 is the only vacuolar aspartic protease and BP2 is the single syntenic ortholog of the two *P. falciparum* DV cysteine endopeptidases, falcipain-2 and 3. The other *Plasmodium* papain-like cysteine endoprotease (FP1 in *P. falciparum*; BP1 in *P. berghei*) is not located in the DV of *P. falciparum* but is located in merozoites and is involved RBC invasion [48]. While the cellular location of both BP1 in *P. berghei* blood stages is unknown, the BP1 ortholog of the closely related rodent parasite *P. yoelii*

(YP1) is also expressed in merozoites and is believed to have a role in RBC invasion [31], suggesting a similar function as FP1. It therefore seems unlikely that BP1 is involved in the initial phase of Hb digestion and release of heme in trophozoite-stage parasites. However, we cannot formally exclude a role for BP1, or indeed another endoprotease, in the initial step of Hb digestion, which would compensate, albeit poorly, for the loss of PM4 and/or BP2. Further research is needed to investigate whether the remaining low-level Hz formation in Δ*pm4*Δ*bp2*-parasites is due to specific cleavage of Hb molecules by other enzymes or results from a non-specific disassembly of the Hb tetramer that may occur either the cytostomes or in the dark-staining vesicles which may be acidified and condensed cytostomes [47].

In *P. falciparum* the plasmepsins and falcipains overlap in function and there is extensive functional redundancy within and between these two protease classes, with the loss of an enzyme being not only being compensated by members of the same protease family but also between the two classes [4,15-17,49,50]. Recently a 200-kDa protein complex has been defined in *P. falciparum* that is required for Hb degradation and Hz formation in the food vacuole [51]. As expected, this protein complex contains the falcipains FP2/2' as well the plasmepsins II–IV in addition to HDP. Interestingly, evidence was provided that FP2 forms a complex with HDP and is involved in Hz formation. Our observations on Hz production in the single gene-deletion mutants Δ*pm4* and Δ*bp2* and the double gene-deletion mutant Δ*pm4*Δ*bp2* indicate that also in *P. berghei* the aspartyl and cysteine endopeptidases overlap in their ability to cleave Hb. Interestingly, the Δ*bp2* mutant, which lacks the FP2 orthologs, has a normal growth rate and produces wt-levels of Hz, whereas Δ*pm4* parasites have a reduced growth and Hz production. These observations demonstrate that while PM4 is able to fully compensate for the function of BP2, BP2 can only partly compensate for the loss of PM4. Moreover, it suggests that BP2 is not necessary for the activation of PM4 as has been suggested previously [49].

The ability of *Plasmodium* parasites to produce mature schizonts without Hz formation may have important implications in the development of drugs that target Hb digestion and for understanding development of resistance against such drugs [40]. We found that Δ*pm4*Δ*bp2*-parasites are less sensitive to chloroquine (CQ) *in vivo.* CQ directly interacts with free heme creating a heme-chloroquine complex that is highly toxic to the parasite [52] and therefore the increased in CQ resistance of Δ*pm4*Δ*bp2* is consistent with our observations of reduced/absent Hb digestion. Interestingly, it has been previously reported that *P. berghei* lines that have been selected for CQ-resistance have a stronger preference for reticulocytes and produce less Hz [53-55]. It has been proposed that CQ-resistance in parasites with reduced Hz is due to detoxification of hemin by elevated

levels of glutathione in parasites that grow inside reticulocytes, thus precluding heme-polymerization and preventing the CQ activity [53,56]. However, our observations may provide a more direct explanation for CQ-resistance and reduced Hz production in these parasites, namely that these parasites digest less Hb in reticulocytes like Δ*pm4*Δ*bp2*-parasites. Despite the reduced sensitivity to CQ, we found that Δ*pm4*Δ*bp2*-parasites disappeared from the blood of mice during continuous CQ treatment (from day 16 after infection with 10^5 parasites). This may be due a combination of factors that characterize Δ*pm4*Δ*bp2* infections in mice. CQ may eliminate the proportion of parasites that still produce (low levels) of Hz thereby slowing the multiplication rate of Δ*pm4*Δ*bp2* parasites and in addition immune responses will limit parasite multiplication in mice. Interestingly, untreated mice also resolve infections between day 15–18, through the removal of iRBC by host immunity. Therefore the eventual drop in a Δ*pm4*Δ*bp2* parasitemia in the CQ-treated mice may not result from CQ action, but from an effectively deployed acquired immune response.

We have been unable to more precisely determine the increase in CQ-resistance of Δ*pm4*Δ*bp2*-parasites *in vitro* since the ring forms of this mutant do not mature into schizonts in culture (see above). While Δ*pm4*Δ*bp2* parasites have an increased resistance to CQ they retain the same sensitivity to artesunate (AS). Although the precise and critical mode of action of artemisinin and related-derivatives remains contentious, most studies concur that their activity results from activation by reduced heme iron in the DV [57,58]. Our results show that compared to wt parasites, Δ*pm4*Δ*bp2*-parasites have a reduced sensitivity to CQ but are equally sensitive to AS. This would suggest that additional, non-heme based, modes of AS action are equally or more effective at targeting *P. berghei* parasites *in vivo*. Therefore, as Δ*pm4*Δ*bp2*-parasites produce little or no Hz they may be useful tools to analyze mode/s of drug action, for example, how inhibitory compounds target and interact with molecules either critical to or result from Hb digestion. The observations on the acquisition of CQ-resistance when parasites develop in reticulocytes with little or no Hz formation may have relevance for *P. vivax*, which is restricted for growth in reticulocytes. Interestingly mechanisms of CQ-resistance in *P. vivax* appear to be different from those in *P. falciparum* [20,59] and no clear association has been found between CQ-resistance in *P. vivax* and mutations associated with CQ-resistance in *P. falciparum*, such as *pfcrt* or *pfmdr1* [20]. Studies into *P. vivax* suggest that development of CQ-resistance also confers cross-resistance to amodiaquine, an anti-malarial that also exercises its effects by complexing with heme [60-62]. Based on our observations, we hypothesize that *P. vivax* may acquire resistance to CQ (and other drugs targeting Hb digestion) by selecting for parasites that have 'switched' to a development mode where they are less dependent on Hb digestion for growth. This 'switching' could be dependent

on genetic (and/or epigenetic) changes that, for example, reduce Hb digestion or increase uptake of amino acids (from the reticulocyte and serum) and thus are unrelated to the genetic changes that influence CQ transport in *P. falciparum* resistant lines [63]. Such 'switching' may only be possible for those *Plasmodium* species that can infect and develop in reticulocytes. It would therefore be of great interest to analyze whether in 'hotspots' of *P. vivax* CQ-resistance parasites have reduced Hz formation.

The ability of *Plasmodium* parasites to develop inside reticulocytes with severely impaired Hb digestion and Hz formation was unexpected given the multiple proposed important roles of Hb digestion for survival in the blood. Our findings support the notion that *Plasmodium* parasites retain multiple modes of development and survival during blood stage development, which has important implications for the development of drugs targeting the *Plasmodium* Hb digestion or Hz formation as well as indicating alternative modes of drug resistance that require further investigation.

Materials and methods

Experimental animals and reference *P. berghei* ANKA lines

Female C57BL/6, BALB/c and Swiss OF1 mice (6–8 weeks old; Charles River/Janvier) were used. All animal experiments performed at the LUMC were approved by the Animal Experiments Committee of the Leiden University Medical Center (DEC 10099; 12042; 12120). All animal experiments performed at the University of Perugia were approved by Ministry of Health under the guidelines D.L. 116/92). The Dutch and Italian Experiments on Animal Act were established under European guidelines (EU directive no. 86/609/EEC regarding the Protection of Animals used for Experimental and Other Scientific Purposes).

Two reference *P. berghei* ANKA parasite lines were used: line cl15cy1 (wt) and reporter line 1037cl1 (wt-GFP-Luc$_{schiz}$; mutant RMgm-32; www.pberghei.eu). This reporter line contains the fusion gene *gfp-luc* gene under control of the schizont-specific *ama1* promoter integrated into the silent *230p* gene locus (PBANKA_030600) and does not contain a drug-selectable marker [18].

Generation of single gene deletion mutants and genotype analyses

Most DNA constructs used to disrupt genes were based on the standard plasmids: plasmid pL0001 (MRA-770, www.mr4.org) and pLTgDFHR both containing the pyrimethamine resistant *Toxoplasma gondii* (*Tg*) dihydrofolate reductase-thymidylate synthase (*dhfr/ts*) as a selectable marker (SM) under the control of the *P. berghei dhfr/ts* promoter;

and plasmid pL0035 (MRA-850, www.mr4.org) containing the h*dhfr*::y*fcu* SM under the control of the *eef1α* promoter [64]. Targeting sequences for homologous recombination were PCR amplified from *P. berghei* ANKA (cl15cy1) genomic DNA using primers specific for the 5' or 3' end of each gene (see Table S1 for the primer sequences). The PCR-amplified target sequences were cloned either upstream or downstream of the SM to allow for integration of the construct into the targeting regions by homologous recombination. The DNA construct targeting *bp1* was kindly provided by Dr. Photini Sinnis (Johns Hopkins University). The DNA deletion constructs were linearized with the appropriate restriction enzymes (Table S1) before transfection.

Several gene deletion constructs were generated by a modified two step PCR method [65]. Briefly, in the first PCR reaction two fragments (5'- and 3'-targeting sequences) of the targeted gene were amplified from *P. berghei* ANKA genomic DNA with the primer sets P1/P2 and P3/P4 (Table S1). Primers P2 and P3 have 5' extensions homologues to the SM cassette. The SM cassette (*eef1α*-h*dfhr*::y*fcu*-3'*dhfr/ts*) was excised by digestion from plasmid pL0048 with *Xho*I and *Not*I [65] or the SM cassette (*eef1α*-h*dfhr*-3'*dhfr/ts*) from plasmid pL0040 with *Xho*I and *Not*I. Primers P1 and P4 have 5' terminal extensions with an anchor-tag suitable for the second PCR reaction. In the second PCR reaction, the amplified 5' and 3' targeting sequences were annealed to either side of the SM cassette, and the joint fragment was amplified by the external anchor-tag primers L4661/L4662, resulting in the PCR-based gene deletion constructs. Before transfection, constructs were digested with appropriate restriction enzymes (in primers P1 and P4, respectively) to remove the 'anchor-tag', and with *Dpn*I to digest any residual plasmids.

Transfection and selection of transformed parasites was performed using standard genetic modification technologies for *P. berghei* [66]. In Table S1 details of all gene-deletion experiments are given such as experiment number, deletion construct and parasite background for transfection. Cloned parasites were obtained from all gene-deletion mutants by the method of limiting dilution. Correct integration of DNA constructs and disruption of genes was verified by diagnostic PCR analyses (see Table S2 for primers) and Southern analyses of chromosomes separated by pulsed-field gel electrophoresis [66]. All information on successfully generated gene deletion mutants and the failed attempts to disrupt genes, including DNA constructs and primers, have been submitted to the RMgmDB database of genetically modified rodent malaria parasites (www.pberghei.eu). The loss of transcripts in gene-deletion mutants was analyzed by standard Northern blot analyses or RT-PCR. Total RNA was isolated from mixed blood-stages of wt *P. berghei* ANKA (cl15cy1) and the different gene-deletion mutant lines. Northern blots were hybridised with probes specific for the open reading frame (ORF) of each gene after PCR

amplification from wt *P. berghei* ANKA genomic DNA (primers shown in Table S2.b). As a loading control, Northern blots were hybridized with the oligonucleotide probe L644R that recognizes the large subunit ribosomal RNA (rRNA) [67]. For RT-PCR primers were designed to amplify a small fragment in the ORF of each gene (primers and product size are shown in Table S3). Amplification of *Pbtub* from cDNA was used as a control (primers and product size are shown in Table S3).

Generation of double gene-deletion mutants and genotype analysis

The Δ*bp2*-b mutant was generated using construct pL1602, which contains the h*dhfr*::y*fcu* SM flanked by two identical 3'UTR *dhfr* sequences [64]. A recombination event between the two 3'UTR *dhfr* sequences results in the removal of the h*dhfr*::y*fcu* SM. Negative selection with 5-fluorocytosine (5-FC) was used to select for parasites that have removed the SM cassette. Mice infected with Δ*bp2*-b parasites were treated with a daily single dose of 0.5 mL of 20 mg/mL drug/day for a period of 4 days starting at a peripheral parasitemia of 0.1–0.5%. Resistant parasites were collected between day 5 and 7 after initiation of the 5-FC treatment, and cloned parasites were obtained by the method of limiting dilution. The genotype of mutant Δ*bp2*-b^{-sm} was analyzed by diagnostic Southern analysis to confirm removal of the h*dhfr*::y*fcu* SM (Figure S4). The gene encoding PM4 was subsequently targeted in this line by standard transfection and drug selection procedures as mentioned above (Figure S4).

In vivo asexual multiplication (growth) rate and virulence of blood-stage parasites

The multiplication (growth) rate of asexual blood-stages in mice was determined during cloning of the gene-deletion mutants as described before [18] and was calculated as follows: the percentage of infected erythrocytes (parasitemia) in Swiss OF1 mice injected with a single parasite was determined by counting Giemsa-stained blood films when parasitemias reach 0.5–2%. The mean asexual multiplication rate per 24 hours was then calculated assuming a total of 1.2×10^{10} erythrocytes per mouse (2mL of blood). The percentage of infected erythrocytes in mice infected with reference lines of the *P. berghei* ANKA strain consistently ranged between 0.5–2% at day 8 after infection, resulting in a mean multiplication rate of 10 per 24 hours [68].

The development of experimental cerebral malaria (ECM) was analyzed in C57BL/6 mice and the course of parasitemia was determined in both BALB/c and C57BL/6 mice. Groups of 5–6 mice were injected intraperitoneally (i.p.) with 10^4–10^5 wt-iRBCs or with 10^5–10^6 mutant-iRBCs (see Results section). The onset of ECM was determined by observation of

clinical signs such as ruffled fur, hunching, wobbly gait, limb paralysis, convulsion, and coma and by measuring the drop in body temperature [18] at day 5 to 8 after infection at 6 hour intervals. The body temperature of infected mice was measured using a laboratory thermometer (model BAT-12, Physitemp Instruments Inc., Clifton, NJ) with a rectal probe (RET-2) for mice. The experiments were terminated when infected mice showed a drop in body temperature below 34°C or showed signs of cerebral complications.

Sizes measurements of parasites inside iRBCs

To measure the sizes of schizonts and gametocytes, tail or cardiac blood containing schizonts was collected from infected BALB/c mice with a high parasitemia (10–30%). Blood was collected in complete RPMI-1640 culture medium. The size of schizonts was determined in fixed iRBC on Giemsa-stained smears and by imagestream flow cytometry of live iRBCs. For the Giemsa-stained smears, pictures were taken using a Leica microscope (1000x magnification; oil immersion) from randomly chosen fields of 300–400 RBCs, and all schizonts and gametocytes were measured in these fields. The sizes of iRBCs and the parasites were measured by ImageJ by gating on the areas of parasites and iRBC. For imagestream flow cytometry analysis, iRBCs containing schizonts of wt-GFP-Luc$_{schiz}$ and Δ*pm4*Δ*bp2*-parasites were first enriched by Nycodenz density centrifugation [66]. Purified parasites were then collected in complete RPMI-1640 culture medium and stained with Hoechst-33258 (2 µmol/L, Sigma, NL) for 1 hour at room temperature. Cultured, mature schizonts of wt *P. berghei* ANKA (cl15cy1) were used as non-staining control; Hoechst stained cl15cy1 (Hoechst only) and non-stained wt-GFP-Luc$_{schiz}$ (GFP only) were used as single-color controls. The analyses were performed using an Amnis ImageStream X imaging cytometer (Amnis Corp.) and images were analyzed using the IDEAS® image analysis software.

Electron microscopy analysis

For electron microscopy analyses, infected blood was collected from wt or Δ*pm4*Δ*bp2* parasite infected BALB/c mice by heart puncture. Infected RBCs were enriched by Nycodenz centrifugation [66]. IRBC (10^7–10^8) were collected and fixed overnight in 2mL of 1.5% glutaraldehyde in 0.1 M sodium cacodylate. After centrifugation, the pellet was rinsed twice with 0.1M sodium cacodylate, and postfixed with 1% osmium tetroxide in 0.1 M sodium cacodylate. After rinsing, samples were dehydrated in a graded ethanol series up to 100% and embedded in Epon. 110-nm sections were cut with a microtome and transferred onto standard grids and post-stained with uranyl acetate and lead citrate. Transmission electron microscopy (TEM) data were collected on a FEI Tecnai microscope

at 120 kV with a FEI Eagle CCD camera. Virtual slides [69] consisting of 759 and 729 unbinned 4kx4k images were collected for the WT and Δ*pm4*Δ*bp2* sample respectively. The magnification at the detector plane was, in both cases, 12930: the pixel size 1.2 nm square. The resulting slides cover an area of $10^9 \times 10^5$ µm^2 and $10^5 \times 10^5$ µm^2 for the respective samples. The virtual slides were analyzed by Aperio ImageScope software (www.aperion.com). All statistical tests were performed using GraphPad Prism.

Quantification of hemozoin in schizonts-iRBC

Hz was quantified in schizonts using different methods. Hz was quantified by measuring the relative light intensity (RLI) of Hz crystals in schizonts by reflection contrast polarized light microscopy [33,70,71]. Schizonts were either collected from overnight *in vitro* blood-stage cultures or directly from tail blood when schizonts were present in the peripheral circulation. For the cultures, infected tail blood (10 µL) with a parasitemia between 0.5 and 1% was cultured overnight in 1mL complete RPMI-1640 culture medium at 37°C under standard conditions for the culture of *P. berghei* blood-stages [35]. Thin blood smears were made from cultured parasites or from tail blood and stained with Hoechst-33342 (2 µmol/L, Sigma, NL) for 20 min. Schizonts (8-24 nuclei) were selected on blood smears based on the Hoechst-stained nuclei and pictures were taken with a LeicaDM/RB microscope (1000x magnification, oil RC immersion objective; Leica, Wetzlar, Germany) which was adapted for RCM as described by Cornetese-ten Velde *et al*. [72]. The RLI of Hz crystals in the schizonts was measured using Image J software.

Quantification of hemozoin in organs

To quantify Hz deposition in organs of infected mice, groups of 8 BALB/c mice were i.p. infected with 10^5 wt, Δ*pm4* or Δ*pm4*Δ*bp2* parasites. At different peripheral parasitemias, mice were sacrificed and systemically perfused with 20 mL PBS to remove circulating iRBC from the organs. Livers, spleens and lungs were removed, weighed and stored at -80°C until further analysis. The Hz extraction from these organs and quantification was performed using an optimized method for Hz quantification in tissues as described [36].

Gametocyte and ookinete production

Gametocyte production is defined as the percentage of ring forms developing into mature gametocytes during synchronized infections [35]. Ookinete production was determined in standard *in vitro* fertilization and ookinete maturation assays and is defined as the

percentage of female gametes that develop into mature ookinetes under standardized *in vitro* culture conditions [73]. Female gamete and mature ookinete numbers were determined on Giemsa-stained blood smears made 16–18 hours post-activation.

Measurement of drug-sensitivity of blood-stage parasites

Groups of 5 BALB/c mice were i.p. infected with either 10^4 wt- or 10^5 Δ*pm4*Δ*bp2*-parasites. At a peripheral parasitemia of 2–5%, mice were treated with artesunate [AS; Pharbaco, Vietnam, 60 mg powder (a kind gift from Dafra Pharma)], chloroquine (CQ; Sigma) or sulfadiazine (SD; Sigma) and peripheral parasitemia was monitored daily by counting Giemsa-stained blood films of tail blood. AS treatment was performed by i.p. injection of 6.25mg/mL in 5% $NaHCO_3$ as a single dose for 4 consecutive days. CQ and SD were provided in the drinking water for a period of 7 days. CQ was provided at a concentration of 288mg/L with 15g/L glucose [74] and SD at a concentration of 35mg/L [75].

Acknowledgements

We would like thank Dr. Photini Sinnis for providing us with a *P. berghei bp1* gene-deletion construct, and Guido de Roo for assistance with flow cytometry experiments. Jing-wen Lin is supported by the China Scholarship Council-Leiden University Joint Program and Chris J. Janse by a grant of the European Community's Seventh Framework Programme (FP7/2007–2013) under grant agreement no. 242095.

References

1. Goldberg DE (2005) Hemoglobin degradation. Curr Top Microbiol Immunol 295: 275-291.
2. Esposito A, Tiffert T, Mauritz JM, Schlachter S, Bannister LH, *et al*. (2008) FRET imaging of hemoglobin concentration in *Plasmodium falciparum*-infected red cells. PLoS One 3: e3780.
3. Sherman IW (1977) Amino acid metabolism and protein synthesis in malarial parasites. Bull World Health Organ 55: 265-276.
4. Liu J, Istvan ES, Gluzman IY, Gross J, Goldberg DE (2006) *Plasmodium falciparum* ensures its amino acid supply with multiple acquisition pathways and redundant proteolytic enzyme systems. Proc Natl Acad Sci U S A 103: 8840-8845.
5. Divo AA, Geary TG, Davis NL, Jensen JB (1985) Nutritional requirements of *Plasmodium falciparum* in culture. I. Exogenously supplied dialyzable components necessary for continuous growth. J Protozool 32: 59-64.
6. Francis SE, Gluzman IY, Oksman A, Knickerbocker A, Mueller R, *et al*. (1994) Molecular characterization and inhibition of a *Plasmodium falciparum* aspartic hemoglobinase. EMBO J 13: 306-317.
7. Babbitt SE, Altenhofen L, Cobbold SA, Istvan ES, Fennell C, *et al*. (2012) *Plasmodium falciparum* responds to amino acid starvation by entering into a hibernatory state. Proc Natl Acad Sci U S A 109: E3278-3287.
8. Elliott DA, McIntosh MT, Hosgood HD, 3rd, Chen S, Zhang G, *et al*. (2008) Four distinct pathways of hemoglobin uptake in the malaria parasite *Plasmodium falciparum*. Proc Natl Acad Sci U S A 105: 2463-2468.
9. Francis SE, Sullivan DJ, Jr., Goldberg DE (1997) Hemoglobin metabolism in the malaria parasite *Plasmodium falciparum*. Annu Rev Microbiol 51: 97-123.
10. Goldberg DE, Slater AF, Beavis R, Chait B, Cerami A, *et al*. (1991) Hemoglobin degradation in the human malaria pathogen *Plasmodium falciparum*: a catabolic pathway initiated by a specific aspartic protease. J Exp Med 173: 961-969.
11. Gluzman IY, Francis SE, Oksman A, Smith CE, Duffin KL, *et al*. (1994) Order and specificity of the *Plasmodium falciparum* hemoglobin degradation pathway. J Clin Invest 93: 1602-1608.
12. Wyatt DM, Berry C (2002) Activity and inhibition of plasmepsin IV, a new aspartic proteinase from the malaria parasite, *Plasmodium falciparum*. FEBS Lett 513: 159-162.
13. Banerjee R, Liu J, Beatty W, Pelosof L, Klemba M, *et al*. (2002) Four plasmepsins are active in the *Plasmodium falciparum* food vacuole, including a protease with an active-site histidine. Proc Natl Acad Sci U S A 99: 990-995.
14. Subramanian S, Hardt M, Choe Y, Niles RK, Johansen EB, *et al*. (2009) Hemoglobin cleavage site-specificity of the *Plasmodium falciparum* cysteine proteases falcipain-2 and falcipain-3. PLoS One 4: e5156.
15. Sijwali PS, Rosenthal PJ (2004) Gene disruption confirms a critical role for the cysteine protease falcipain-2 in hemoglobin hydrolysis by *Plasmodium falciparum*. Proc Natl Acad Sci U S A 101: 4384-4389.
16. Bonilla JA, Bonilla TD, Yowell CA, Fujioka H, Dame JB (2007) Critical roles for the digestive vacuole plasmepsins of *Plasmodium falciparum* in vacuolar function. Mol Microbiol 65: 64-75.

17. Omara-Opyene AL, Moura PA, Sulsona CR, Bonilla JA, Yowell CA, *et al*. (2004) Genetic disruption of the *Plasmodium falciparum* digestive vacuole plasmepsins demonstrates their functional redundancy. J Biol Chem 279: 54088-54096.

18. Spaccapelo R, Aime E, Caterbi S, Arcidiacono P, Capuccini B, *et al*. (2011) Disruption of plasmepsin-4 and merozoites surface protein-7 genes in *Plasmodium berghei* induces combined virulence-attenuated phenotype. Sci Rep 1: 39.

19. Baird JK (2004) Chloroquine resistance in *Plasmodium vivax*. Antimicrob Agents Chemother 48: 4075-4083.

20. Baird KJ, Maguire JD, Price RN (2012) Diagnosis and treatment of *Plasmodium vivax* malaria. Adv Parasitol 80: 203-270.

21. Singh A, Walker KJ, Sijwali PS, Lau AL, Rosenthal PJ (2007) A chimeric cysteine protease of *Plasmodium berghei* engineered to resemble the *Plasmodium falciparum* protease falcipain-2. Protein Eng Des Sel 20: 171-177.

22. Ponpuak M, Klemba M, Park M, Gluzman IY, Lamppa GK, *et al*. (2007) A role for falcilysin in transit peptide degradation in the *Plasmodium falciparum* apicoplast. Mol Microbiol 63: 314-334.

23. Klemba M, Gluzman I, Goldberg DE (2004) A *Plasmodium falciparum* dipeptidyl aminopeptidase I participates in vacuolar hemoglobin degradation. J Biol Chem 279: 43000-43007.

24. Ragheb D, Bompiani K, Dalal S, Klemba M (2009) Evidence for catalytic roles for *Plasmodium falciparum* aminopeptidase P in the food vacuole and cytosol. J Biol Chem 284: 24806-24815.

25. Dalal S, Klemba M (2007) Roles for two aminopeptidases in vacuolar hemoglobin catabolism in *Plasmodium falciparum*. J Biol Chem 282: 35978-35987.

26. Ragheb D, Dalal S, Bompiani KM, Ray WK, Klemba M (2011) Distribution and biochemical properties of an M1-family aminopeptidase in *Plasmodium falciparum* indicate a role in vacuolar hemoglobin catabolism. J Biol Chem 286: 27255-27265.

27. Stack CM, Lowther J, Cunningham E, Donnelly S, Gardiner DL, *et al*. (2007) Characterization of the *Plasmodium falciparum* M17 leucyl aminopeptidase. A protease involved in amino acid regulation with potential for antimalarial drug development. J Biol Chem 282: 2069-2080.

28. Jani D, Nagarkatti R, Beatty W, Angel R, Slebodnick C, *et al*. (2008) HDP-a novel heme detoxification protein from the malaria parasite. PLoS Pathog 4: e1000053.

29. Sijwali PS, Koo J, Singh N, Rosenthal PJ (2006) Gene disruptions demonstrate independent roles for the four falcipain cysteine proteases of *Plasmodium falciparum*. Mol Biochem Parasitol 150: 96-106.

30. Sijwali PS, Kato K, Seydel KB, Gut J, Lehman J, *et al*. (2004) *Plasmodium falciparum* cysteine protease falcipain-1 is not essential in erythrocytic stage malaria parasites. Proc Natl Acad Sci U S A 101: 8721-8726.

31. Kumar A, Kumar K, Korde R, Puri SK, Malhotra P, *et al*. (2007) Falcipain-1, a *Plasmodium falciparum* cysteine protease with vaccine potential. Infect Immun 75: 2026-2034.

32. Arastu-Kapur S, Ponder EL, Fonovic UP, Yeoh S, Yuan F, *et al*. (2008) Identification of proteases that regulate erythrocyte rupture by the malaria parasite *Plasmodium falciparum*. Nat Chem Biol 4: 203-213.

33. Maude RJ, Buapetch W, Silamut K (2009) A simplified, low-cost method for polarized light microscopy. Am J Trop Med Hyg 81: 782-783.

34. Lawrence C, Olson JA (1986) Birefringent hemozoin identifies malaria. Am J Clin Pathol 86: 360-363.

35. Janse CJ, Waters AP (1995) *Plasmodium berghei*: the application of cultivation and purification techniques to molecular studies of malaria parasites. Parasitol Today 11: 138-143.

36. Deroost K, Lays N, Noppen S, Martens E, Opdenakker G, *et al*. (2012) Improved methods for haemozoin quantification in tissues yield organ-and parasite-specific information in malaria-infected mice. Malar J 11: 166.

37. Egan TJ, Koch KR, Swan PL, Clarkson C, Van Schalkwyk DA, *et al*. (2004) *In vitro* antimalarial activity of a series of cationic 2,2'-bipyridyl- and 1,10-phenanthrolineplatinum(II) benzoylthiourea complexes. J Med Chem 47: 2926-2934.

38. Klonis N, Crespo-Ortiz MP, Bottova I, Abu-Bakar N, Kenny S, *et al*. (2011) Artemisinin activity against *Plasmodium falciparum* requires hemoglobin uptake and digestion. Proc Natl Acad Sci U S A 108: 11405-11410.

39. Kinnamon KE, Ager AL, Orchard RW (1976) *Plasmodium berghei*: combining folic acid antagonists for potentiation against malaria infections in mice. Exp Parasitol 40: 95-102.

40. Tilley L, Dixon MW, Kirk K (2011) The *Plasmodium falciparum*-infected red blood cell. Int J Biochem Cell Biol 43: 839-842.

41. Lew VL, Tiffert T, Ginsburg H (2003) Excess hemoglobin digestion and the osmotic stability of *Plasmodium falciparum*-infected red blood cells. Blood 101: 4189-4194.

42. Krugliak M, Zhang J, Ginsburg H (2002) Intraerythrocytic *Plasmodium falciparum* utilizes only a fraction of the amino acids derived from the digestion of host cell cytosol for the biosynthesis of its proteins. Mol Biochem Parasitol 119: 249-256.

43. Ginsburg H (1990) Some reflections concerning host erythrocyte-malarial parasite interrelationships. Blood Cells 16: 225-235.

44. Koury MJ, Koury ST, Kopsombut P, Bondurant MC (2005) *In vitro* maturation of nascent reticulocytes to erythrocytes. Blood 105: 2168-2174.

45. Allen DW (1960) Amino acid accumulation by human reticulocytes. Blood 16: 1564-1571.

46. Vaid A, Ranjan R, Smythe WA, Hoppe HC, Sharma P (2010) PfPI3K, a phosphatidylinositol-3 kinase from *Plasmodium falciparum*, is exported to the host erythrocyte and is involved in hemoglobin trafficking. Blood 115: 2500-2507.

47. Fitch CD, Cai GZ, Chen YF, Ryerse JS (2003) Relationship of chloroquine-induced redistribution of a neutral aminopeptidase to hemoglobin accumulation in malaria parasites. Arch Biochem Biophys 410: 296-306.

48. Greenbaum DC, Baruch A, Grainger M, Bozdech Z, Medzihradszky KF, *et al*. (2002) A role for the protease falcipain 1 in host cell invasion by the human malaria parasite. Science 298: 2002-2006.

49. Drew ME, Banerjee R, Uffman EW, Gilbertson S, Rosenthal PJ, *et al*. (2008) *Plasmodium* food vacuole plasmepsins are activated by falcipains. J Biol Chem 283: 12870-12876.

50. Rosenthal PJ, McKerrow JH, Aikawa M, Nagasawa H, Leech JH (1988) A malarial cysteine proteinase is necessary for hemoglobin degradation by *Plasmodium falciparum*. J Clin Invest 82: 1560-1566.

51. Chugh M, Sundararaman V, Kumar S, Reddy VS, Siddiqui WA, *et al*. (2013) Protein complex directs hemoglobin-to-hemozoin formation in *Plasmodium falciparum*. Proc Natl Acad Sci U S A 110: 5392-5397.

52. Fitch CD (1986) Antimalarial schizontocides: ferriprotoporphyrin IX interaction hypothesis. Parasitol Today 2: 330-331.

53. Platel DF, Mangou F, Tribouley-Duret J (1999) Role of glutathione in the detoxification of ferriprotoporphyrin IX in chloroquine resistant *Plasmodium berghei*. Mol Biochem Parasitol 98: 215-223.

54. Peters W (1968) The chemotherapy of rodent malaria. VII. The action of some sulphonamides alone or with folic reductase inhibitors against malaria vectors and parasites, 2: schizontocidal action in the albino mouse. Annu Rev Pharmacol 64: 488-494.

55. Peters W (1968) The chemotherapy of rodent malaria. V. Dynamics of drug resistance. I. Methods for studying the acquisition and loss of resistance to chloroquine by Plasmodiun *berghei*. Ann Trop Med Parasitol 62: 277 -287.

56. Fidock M, DeSilva B (2012) Bioanalysis of biomarkers for drug development. Bioanalysis 4: 2425-2426.

57. Eastman RT, Fidock DA (2009) Artemisinin-based combination therapies: a vital tool in efforts to eliminate malaria. Nat Rev Microbiol 7: 864-874.

58. Olliaro PL, Haynes RK, Meunier B, Yuthavong Y (2001) Possible modes of action of the artemisinin-type compounds. Trends Parasitol 17: 122-126.

59. Suwanarusk R, Russell B, Chavchich M, Chalfein F, Kenangalem E, *et al*. (2007) Chloroquine resistant *Plasmodium vivax*: *in vitro* characterisation and association with molecular polymorphisms. PLoS One 2: e1089.

60. Hasugian AR, Tjitra E, Ratcliff A, Siswantoro H, Kenangalem E, *et al*. (2009) *In vivo* and *in vitro* efficacy of amodiaquine monotherapy for treatment of infection by chloroquine-resistant *Plasmodium vivax*. Antimicrob Agents Chemother 53: 1094-1099.

61. Hasugian AR, Purba HL, Kenangalem E, Wuwung RM, Ebsworth EP, *et al*. (2007) Dihydroartemisinin-piperaquine versus artesunate-amodiaquine: superior efficacy and posttreatment prophylaxis against multidrug-resistant *Plasmodium falciparum* and *Plasmodium vivax* malaria. Clin Infect Dis 44: 1067-1074.

62. Russell B, Chalfein F, Prasetyorini B, Kenangalem E, Piera K, *et al*. (2008) Determinants of *in vitro* drug susceptibility testing of *Plasmodium vivax*. Antimicrob Agents Chemother 52: 1040-1045.

63. Ecker A, Lehane AM, Clain J, Fidock DA (2012) PfCRT and its role in antimalarial drug resistance. Trends Parasitol 28: 504-514.

64. Braks JA, Franke-Fayard B, Kroeze H, Janse CJ, Waters AP (2006) Development and application of a positive-negative selectable marker system for use in reverse genetics in *Plasmodium*. Nucleic Acids Res 34: e39.

65. Lin JW, Annoura T, Sajid M, Chevalley-Maurel S, Ramesar J, *et al*. (2011) A novel 'gene insertion/marker out' (GIMO) method for transgene expression and gene complementation in rodent malaria parasites. PLoS One 6: e29289.

66. Janse CJ, Ramesar J, Waters AP (2006) High-efficiency transfection and drug selection of genetically transformed blood stages of the rodent malaria parasite *Plasmodium berghei*. Nat Protoc 1: 346-356.

67. van Spaendonk RM, Ramesar J, van Wigcheren A, Eling W, Beetsma AL, *et al*. (2001) Functional equivalence of structurally distinct ribosomes in the malaria parasite, *Plasmodium berghei*. J Biol Chem 276: 22638-22647.

68. Janse CJ, Haghparast A, Speranca MA, Ramesar J, Kroeze H, *et al*. (2003) Malaria parasites lacking eef1a have a normal S/M phase yet grow more slowly due to a longer G1 phase. Mol Microbiol 50: 1539-1551.

69. Faas FG, Avramut MC, van den Berg BM, Mommaas AM, Koster AJ, *et al*. (2012) Virtual nanoscopy: generation of ultra-large high resolution electron microscopy maps. J Cell Biol 198: 457-469.

70. Prins FA, van Diemen-Steenvoorde R, Bonnet J, Cornelese-ten Velde I (1993) Reflection contrast microscopy of ultrathin sections in immunocytochemical localization studies: a versatile technique bridging electron microscopy with light microscopy. Histochemistry 99: 417-425.

71. Prins FA, Velde IC, de Heer E (2006) Reflection contrast microscopy: The bridge between light and electron microscopy. Methods Mol Biol 319: 363-401.

72. Cornelese-ten Velde I, Bonnet J, Tanke HJ, Ploem JS (1988) Reflection contrast microscopy. Visualization of (peroxidase-generated) diaminobenzidine polymer products and its underlying optical phenomena. Histochemistry 89: 141-150.

73. van Dijk MR, Janse CJ, Thompson J, Waters AP, Braks JA, *et al*. (2001) A central role for P48/45 in malaria parasite male gamete fertility. Cell 104: 153-164.

74. Lewis MD, Pfeil J, Mueller AK (2011) Continuous oral chloroquine as a novel route for *Plasmodium* prophylaxis and cure in experimental murine models. BMC Res Notes 4: 262.

75. Beetsma AL, van de Wiel TJ, Sauerwein RW, Eling WM (1998) *Plasmodium berghei* ANKA: purification of large numbers of infectious gametocytes. Exp Parasitol 88: 69-72.

76. Liu J, Gluzman IY, Drew ME, Goldberg DE (2005) The role of *Plasmodium falciparum* food vacuole plasmepsins. J Biol Chem 280: 1432-1437.

77. Bonilla JA, Moura PA, Bonilla TD, Yowell CA, Fidock DA, *et al*. (2007) Effects on growth, hemoglobin metabolism and paralogous gene expression resulting from disruption of genes encoding the digestive vacuole plasmepsins of *Plasmodium falciparum*. Int J Parasitol 37: 317-327.

78. Klemba M, Beatty W, Gluzman I, Goldberg DE (2004) Trafficking of plasmepsin II to the food vacuole of the malaria parasite *Plasmodium falciparum*. J Cell Biol 164: 47-56.

79. Dahl EL, Rosenthal PJ (2005) Biosynthesis, localization, and processing of falcipain cysteine proteases of *Plasmodium falciparum*. Mol Biochem Parasitol 139: 205-212.

80. Dasaradhi PV, Korde R, Thompson JK, Tanwar C, Nag TC, *et al*. (2007) Food vacuole targeting and trafficking of falcipain-2, an important cysteine protease of human malaria parasite *Plasmodium falciparum*. Mol Biochem Parasitol 156: 12-23.

81. Rosenthal PJ (2011) Falcipains and other cysteine proteases of malaria parasites. Adv Exp Med Biol 712: 30-48.

82. Lamarque M, Tastet C, Poncet J, Demettre E, Jouin P, *et al*. (2008) Food vacuole proteome of the malarial parasite *Plasmodium falciparum*. Proteomics Clin Appl 2: 1361-1374.

Supplementary Material

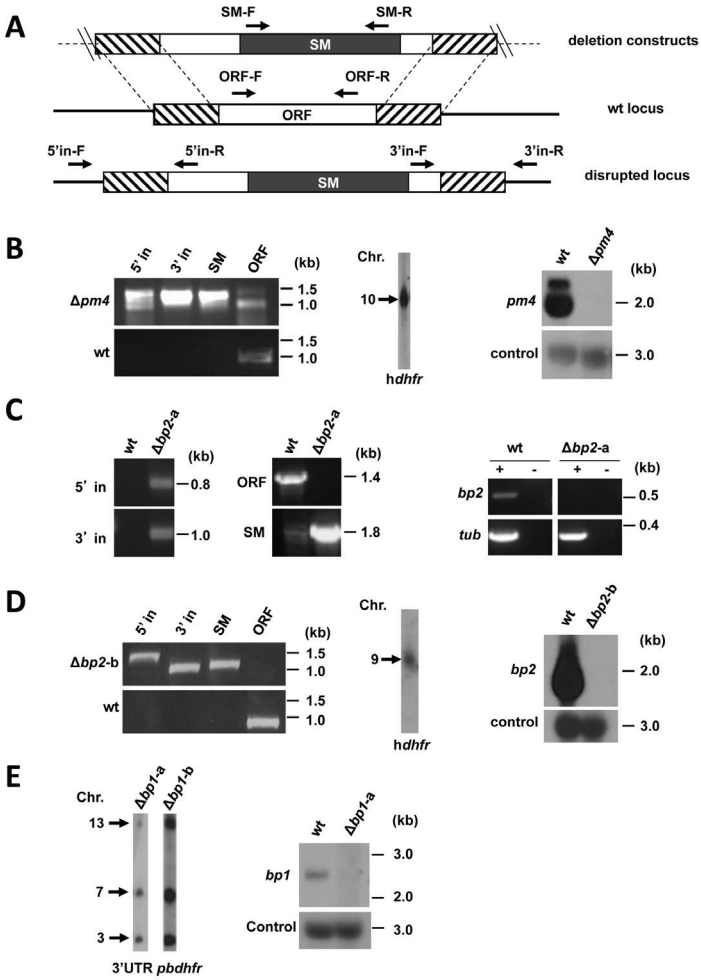

Figure S1. Generation of the *P. berghei* mutants Δ*pm4*, Δ*bp1* and Δ*bp2*.

A. Schematic representation of gene-deletion constructs targeting the open reading frame (ORF) of genes expressing plasmepsin 4 (*pm4*), berghepain 2 (*bp2*) or berghepain 1 (*bp1*) by double cross-over homologous recombination, and wild-type (wt) gene loci before and after disruption. The constructs contain a drug-selectable marker cassette (SM; black box) and gene target regions (hatched boxes). See Table S2 for primer sequences used to amplify the target regions. Primer positions (arrows) for diagnostic PCRs are shown (see Table S3 for primer sequences and expected product sizes).

B. Diagnostic PCR (left) and Southern analysis of pulsed field gel-separated chromosomes (center) confirm correct disruption of *pm4* in mutant Δ*pm4*-b. Northern analysis of blood-stage mRNA (right) confirms the absence of *pm4* transcripts in the Δ*pm4*-b mutant. The following primers were used for diagnostic PCRs: 5' integration (5' in): L5516/L4096; 3' integration: (3' in) L1662/L5517; SM (h*dfhr*::y*fcu*): L4698/L4699; *pm4* ORF: L5518/L5519. Separated chromosomes were hybridized using an h*dhfr* probe that recognizes the DNA-construct integrated into the *pm4* locus on chromosome 10. Northern blot was hybridized using a PCR probe

recognizing the *pm4* ORF (primers L5518/L5519) and with an oligonucleotide probe L644R recognizing the large subunit rRNA (as loading control).

C. Diagnostic PCR (left) confirms the correct deletion of the *bp2* gene in mutant Δ*bp2*-a. RT-PCR analysis of blood stage mRNA (right) shows the absence of *bp2* transcription in Δ*bp2*-a blood-stages. The following primer pairs were used for diagnostic PCR analyses: 5' in, RS835/RS32; 3' in, RS110/RS836; SM (*tgdhfr*/*ts*), RS404/RS405; *bp2* ORF, RS514/RS515. For RT-PCR the following primers were used: tub (*tubulin*), RS782/RS783 and *bp2*, RS515/RS516.

D. Diagnostic PCR (left) and Southern analysis of pulsed field gel-separated chromosomes (center) confirm the correct disruption of the *bp2* gene in mutant Δ*bp2*-b. Northern blot analysis of blood stage mRNA (right) confirms the absence of *bp2* transcripts in Δ*bp2*-b. The following primers were used for diagnostic PCRs: 5' in, L5024/L3211; 3' in, L5025/L1662; SM (h*dhfr*::y*fcu*), L4698/L4699; *bp2* ORF, L5026/L5027. Separated chromosomes were hybridized using an h*dhfr* probe that recognizes the DNA-construct integrated into the *bp2* locus on chromosome 9. Northern blot was hybridized using a PCR probe recognizing the *bp2* ORF (primers L5026/L5027) and with an oligonucleotide probe L644R recognizing the large subunit rRNA (as loading control).

E. Southern analysis of pulsed field gel-separated chromosomes (left) confirms the correct disruption of *bp1* in mutant Δ*bp1*-a and Δ*bp1*-b. Northern analysis of blood-stage mRNA (right) confirms the absence of *bp1* transcripts in mutant Δ*bp1*-a. Separated chromosomes were hybridized using an 3'UTR *pbdhfr* probe that recognizes the DNA-construct integrated into the *bp1* locus on chromosome 13, the endogenous *dhfr*/*ts* on chromosome 7 and the GFP-luciferase reporter cassette in the *230p* locus on chromosome 3. Northern blot was hybridized using a PCR probe recognizing the *bp1* ORF (primers L7422/L7423) and with an oligonucleotide probe L644R recognizing the large subunit rRNA (as loading control). See Table S3 for primers used for generation of probes.

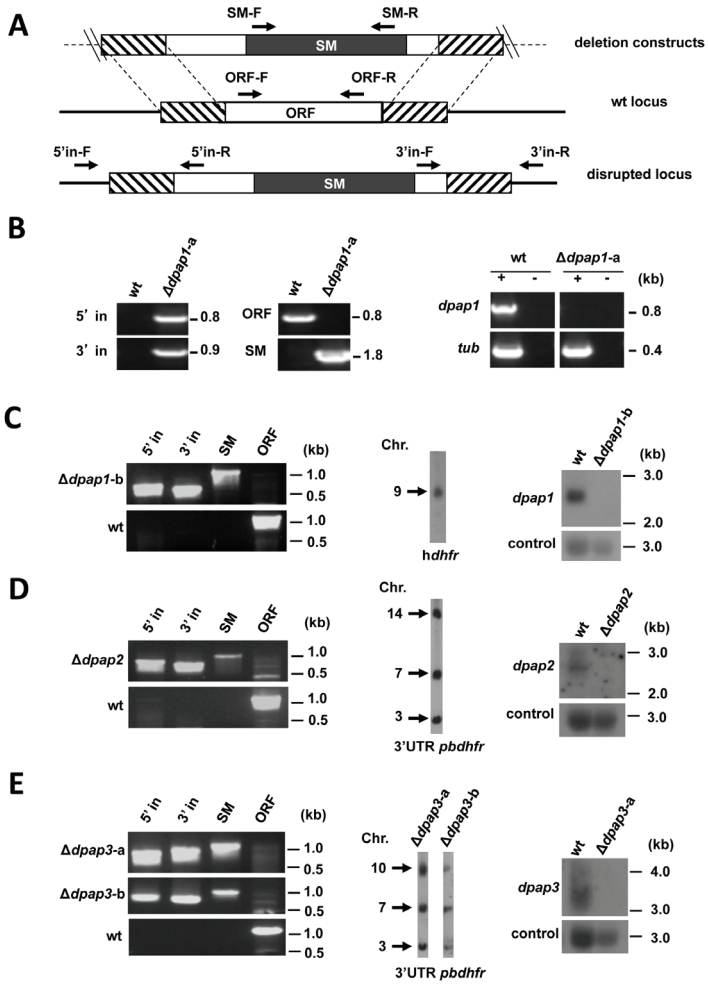

Figure S2. Generation of the *P. berghei* mutants Δ*dpap1*, Δ*dpap2* and Δ*dpap3*.

A. Schematic representation of the gene-deletion constructs targeting the ORF of genes expressing dipeptidyl peptidases 1-3 (*dpap1-3*) by double cross-over homologous recombination and the wt gene loci before and after disruption. The constructs contain a drug-selectable marker cassette (SM; black box) and gene target regions (hatched boxes). See Table S2 for primer sequences used to amplify the target regions. Primer positions (arrows) for diagnostic PCRs are shown (see Table S3 for primer sequences and expected product sizes).

B. Diagnostic PCR (left, center) and RT-PCR (right) analysis confirm correct disruption of *dpap1* in Δ*dpap1*-a. For diagnostic PCRs, the following primers were used: 5' in, RS672/RS32; 3' in, RS110/RS673; SM (*tgdhfr/ts*), RS404/RS405; *dpap1* ORF, RS582/RS583. For RT-PCR the following primers were used: tub (*tubulin*), RS782/RS783 and *dpap1*, RS582/RS583.

C. Diagnostic PCR (left) and Southern analysis of pulsed field gel-separated (center) confirm correct disruption of *dpap1* in Δ*dpap1*-b. Northern analysis of blood-stage mRNA (right) confirms the absence of *dpap1* transcripts in the Δ*dpap1*-b mutant. The following primers were used for diagnostic PCRs: 5' integration (5' in), L6204/L4770; 3' integration (3' in), L4771/L6205; SM (h*dfhr*::y*fcu*), L4698/L4699; *dpap1* ORF, L6206/L6207. For Southern analysis, separated chromosomes were hybridized using an h*dhfr* probe that recognizes the construct integrated into the *dpap1* locus on chromosome 9. Northern blot was hybridized using a PCR probe recognizing

the *dpap1* ORF (primers L6206/L6207). As a loading control, hybridization was performed with oligonucleotide probe L644R that recognizes the large subunit rRNA.

D. Diagnostic PCR (left) and Southern analysis of pulsed field gel-separated chromosomes (center) confirms correct disruption of *dpap2* in mutant Δ*dpap2*. Northern analysis of blood-stage mRNA (right) confirms the absence of *dpap2* transcripts in the Δ*dpap2* mutant. The following primers were used for diagnostic PCRs: 5' in, L6935/L4770; 3' in, L4771/L6936; SM (h*dfhr*::y*fcu*), L4698/L4699; *dpap2* ORF, L6937/L6938. Separated chromosomes were hybridized using a 3'UTR *pbdhfr* probe that recognizes the construct integrated into *dpap2* on chromosome 14, the endogenous *dhfr*/*ts* on chromosome 7 and the GFP-luciferase reporter cassette in the *230p* locus on chromosome 3. Northern blot was hybridized using a PCR probe recognizing the *dpap2* ORF (primers L6937/L6938) and with an oligonucleotide probe L644R recognizing the large subunit rRNA (as loading control).

E. Diagnostic PCR (left) and Southern analysis of pulsed field gel-separated chromosomes (center) confirm correct disruption of *dpap3* in Δ*dpap3*-a and Δ*dpap3*-b. Northern analysis of blood-stage mRNA (right) confirms the absence of *dpap3* transcripts. The following primers were used for diagnostic PCRs: 5' in, L6941/L4770; 3' in, L4771/L6942; SM (h*dfhr*::y*fcu*), L4698/L4699; *dpap3* ORF, L6943/L6944. Separated chromosomes were hybridized using a 3'UTR *pbdhfr* probe that recognizes the construct integrated into *dpap3* on chromosome 10, the endogenous *dhfr*/*ts* on chromosome 7 and the GFP-luciferase reporter cassette in the *230p* locus on chromosome 3. Northern blot was hybridized using a PCR probe recognizing the *dpap3* ORF (primers L6943/L6944) and with an oligonucleotide probe L644R recognizing the large subunit rRNA (as loading control). See Table S3 for primers used for generation of probes.

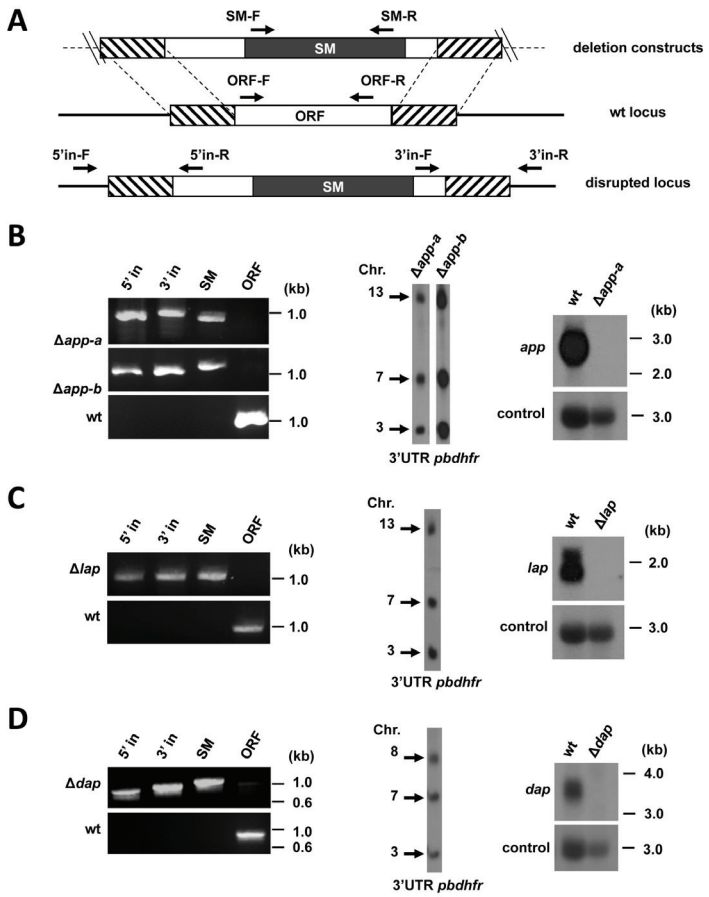

Figure S3. Generation of *P. berghei* mutants Δ*app*, Δ*lap* and Δ*dap*.

A. Schematic representation of the gene-deletion constructs targeting the ORF of genes expressing *aminopeptidase P* (*app*), leucyl aminopeptidase (*lap*) and aspartyl aminopeptidase (*dap*) by double cross-over homologous recombination and the wt gene loci before and after disruption. The constructs contain a drug-selectable marker cassette (SM; black box) and gene target regions (hatched boxes). See Table S2 for primer sequences used to amplify the target regions. Primer positions (arrows) for diagnostic PCRs are shown (see Table S3 for primer sequences and expected product sizes).

B. Diagnostic PCR (left) and Southern analysis of pulsed field gel-separated chromosomes (center) confirm correct disruption of *app* in Δ*app*-a and Δ*app*-b. Northern analysis of blood-stage mRNA (right) confirms the absence of the *app* transcripts in the Δ*app* mutants. The following primers were used for diagnostic PCRs: 5' integration (5' in): L7107/L4770; 3' integration (3' in): L4771/L7108; SM (h*dfhr*::y*fcul*): L4698/L4699; *app* ORF: L7109/L7110. Separated chromosomes of Δ*app*-a and Δ*app*-b were hybridized using a 3'UTR *pbdhfr* probe that recognizes the construct integrated into the *app* locus on chromosome 13, the endogenous *dhfr*/*ts* on chromosome 7 and the GFP-luciferase reporter cassette in the *230p* locus on chromosome 3. Northern blot was hybridized using a PCR probe recognizing the *app* ORF (primers L7109/L7110) and with an oligonucleotide probe L644R recognizing the large subunit rRNA (as loading control).

C. Diagnostic PCR (left) and Southern analysis of separated chromosomes (center) confirm correct disruption of *lap* in mutant Δ*lap*. Northern analysis of blood-stage mRNA (right) confirms the absence of *lap* transcripts in

the Δ*lap* mutant. The following primers were used for diagnostic PCRs: 5' in, L6967/L4770; 3' in, L4771/L6968; SM (h*dfhr*::y*fcu*), L4698/L4699; *lap* ORF, L6969/L6970. Separated chromosomes were hybridized using a 3'UTR *pbdhfr* probe that recognizes the construct integrated into *lap* on chromosome 13, the endogenous *dhfr*/*ts* on chromosome 7 and the GFP-luciferase reporter cassette in the *230p* locus on chromosome 3. Northern blot was hybridized using a PCR probe recognizing *lap* ORF (primers L6969/L6970) and with an oligonucleotide probe L644R recognizing the large subunit rRNA (as loading control).

D. Diagnostic PCR (left) and Southern analysis of pulsed field gel-separated chromosomes (center) confirm correct disruption of *dap* in Δ*dap.* Northern analysis of blood-stage mRNA (right) confirms the absence of the *dap* transcripts in the Δ*dap* mutant. The following primers were used for diagnostic PCRs: 5' in, L6975/L4770; 3' in, L4771/L6976; SM (h*dfhr*::y*fcu*), L4698/L4699; *dap* ORF, L6977/L6978. Separated chromosomes were hybridized using a 3'UTR *pbdhfr* probe that recognizes the construct integrated into *dap* on chromosome 8, the endogenous *dhfr*/*ts* on chromosome 7 and the GFP-luciferase reporter cassette in the *230p* locus on chromosome 3. For Northern blot was hybridized using a PCR probe recognizing *dap* ORF (primers L6977/L6978) and with an oligonucleotide probe L644R recognizing the large subunit rRNA (as loading control). See Table S3 for primers used for generation of probes.

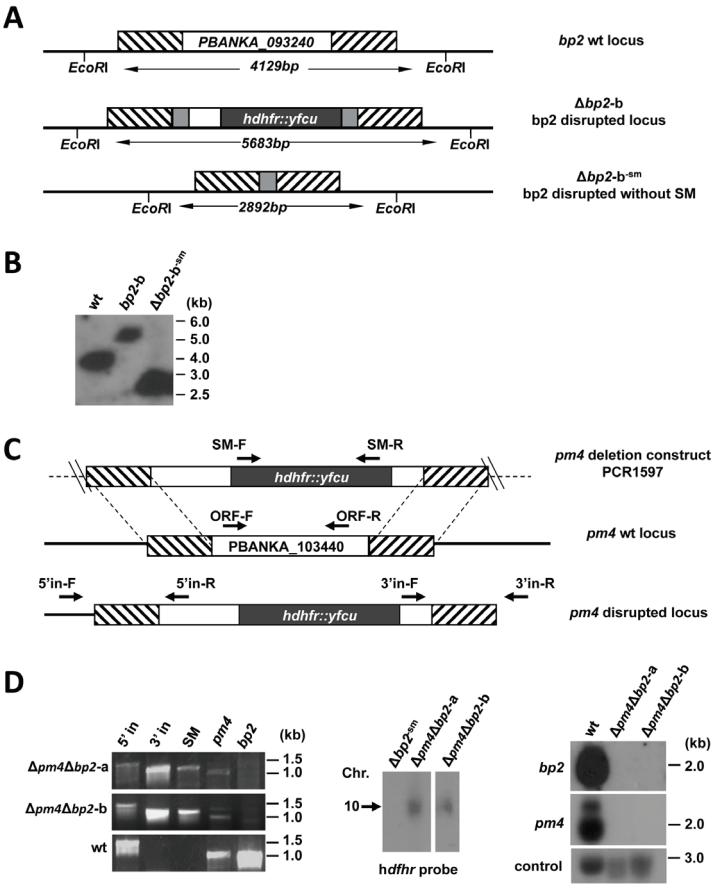

Figure S4. Generation of two independent *P. berghei* Δ*pm4*Δ*bp2* mutants

A. Schematic representation of the wt berghepain 2 (*bp2*) gene locus, the disrupted *bp2* locus in mutant

deletion Δ*bp2*-b and the locus of Δ*bp2*-b^{-sm}. In the Δ*bp2*-b^{-sm} the drug selectable marker (SM, black) has been removed by negative selection using 5-FC. Construct pL1602, used to generate mutant Δ*bp2*-b, targets *bp2* by double cross-over homologous recombination at the target regions (hatched boxes) and contains a positive-negative SM (h*dhfr*::y*fcu*) flanked on both sides by 3'*pbdhfr* sequences (grey boxes). The application of negative selection (5-FC) on Δ*bp2*-b parasites permits the selection of Δ*bp2*-b^{-sm} parasites without the SM that has been excised from the genome as a result of a recombination event between the two 3'*pbdhfr* sequences. Restriction sites and size of the expected fragments in Southern analysis (see B) are shown.

B. Southern analysis of *Eco*RI digested DNA of wt, Δ*bp2*-b and Δ*bp2*-b^{-sm} parasites, confirming correct integration of construct pL1602 in Δ*bp2*-b and the subsequent removal of the SM cassette in Δ*bp2*-b^{-sm} after negative selection (see **A** for the expected sizes of the *Eco*RI fragments). Hybridization was performed using a probe recognizing 3'UTR of *bp2* (primers L5460/L5461).

C. Schematic representation of the gene-deletion construct targeting the ORF of plasmepsin 4 (*pm4*) by double cross-over homologous recombination and the wt gene locus before and after disruption. The constructs contain a drug-selectable marker cassette (SM; black box) and gene target regions (hatched boxes). See Table S2 for primer sequences used to amplify the target regions. Primer positions (arrows) for diagnostic PCRs are shown. See Table S3for primer sequences and expected product sizes.

D. Diagnostic PCR (left) and Southern analysis of separated chromosomes (center) confirm correct disruption of *pm4* and *bp2* in Δ*pm4*Δ*bp2*-a and Δ*pm4*Δ*bp2*-b. Northern analysis of blood-stage mRNA (right) confirms the absence of transcripts of *pm4* and *bp2* in the mutants. The following primers were used for diagnostic PCRs: 5' integration (5' in): L5516/L4096; 3' integration (3' in): L1662/L5517; SM (h*dfhr*::y*fcu*): L4698/L4699; *pm4* ORF: L5518/L5519; *bp2* ORF: L5026/L5027. Separated chromosomes were hybridized using an h*dhfr* probe that recognizes the construct integrated into *pm4* on chromosome 10. Northern blots were hybridized using a PCR probe recognizing the *bp2* ORF (primers L5026/L5027) or the *pm4* ORF (primers L5518/L5519) and with an oligonucleotide probe L644R recognizing the large subunit rRNA (as loading control). See Table S3 for primers used for generation of the probes.

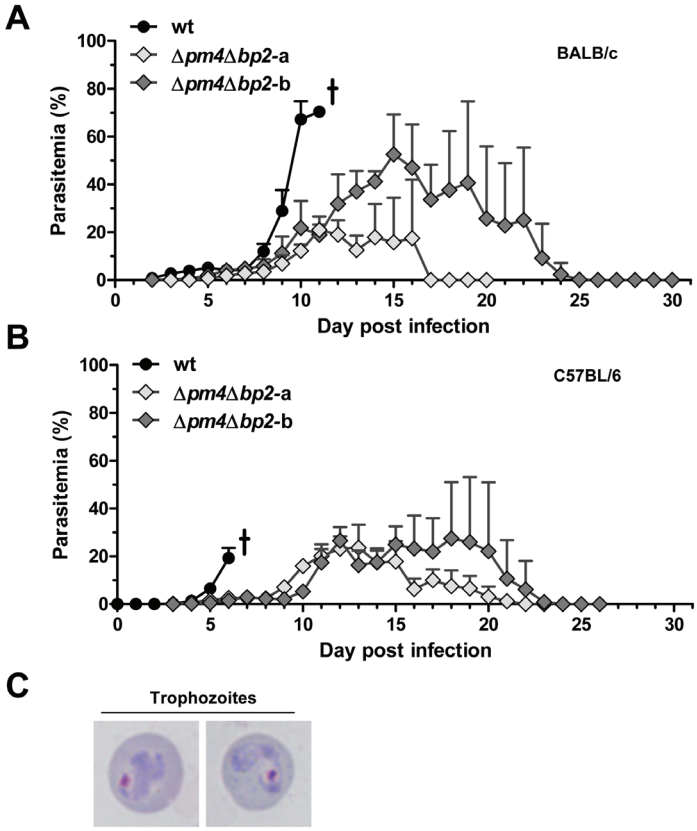

Figure S5. Δ*pm4*Δ*bp2* parasites cause self-resolving blood infections in both C57BL/6 and BALB/c mice

A. Course of parasitemia in BALB/c mice. Mice (n=6) were intraperitoneally (i.p) infected with 10^5 wt, 10^5 Δ*pm4*Δ*bp2*-a or 10^6 Δ*pm4*Δ*bp2*-b parasites. Wt-infected mice developed hyperparasitemia and severe anemia in the second week post infection (p.i) and were sacrificed on day 10-11 p.i. Mice infected with Δ*pm4*Δ*bp2*-parasites resolved infections resulting in undetectable parasitemia by microscopic analysis between day 17 and 25 after infection.

B. Course of parasitemia inC57BL/6 mice. Mice (n=6) were i.p infected with 10^5 wt, 10^5 Δ*pm4*Δ*bp2*-a or 10^6 Δ*pm4*Δ*bp2*-b parasites. All wt-infected mice developed cerebral complications at day 6 after infection, whereas none of the mice infected with Δ*pm4*Δ*bp2*-a or Δ*pm4*Δ*bp2*-b parasites developed ECM. Mice infected with Δ*pm4*Δ*bp2* parasites resolved infections resulting in undetectable parasitemia by microscopic analysis between day 22 and 24 after infection.

C. Trophozoites of Δ*pm4*Δ*bp2*-parasites on Giemsa-stained blood smears showing translucent vesicles in the cytoplasm and the absence of hemozoin pigment.

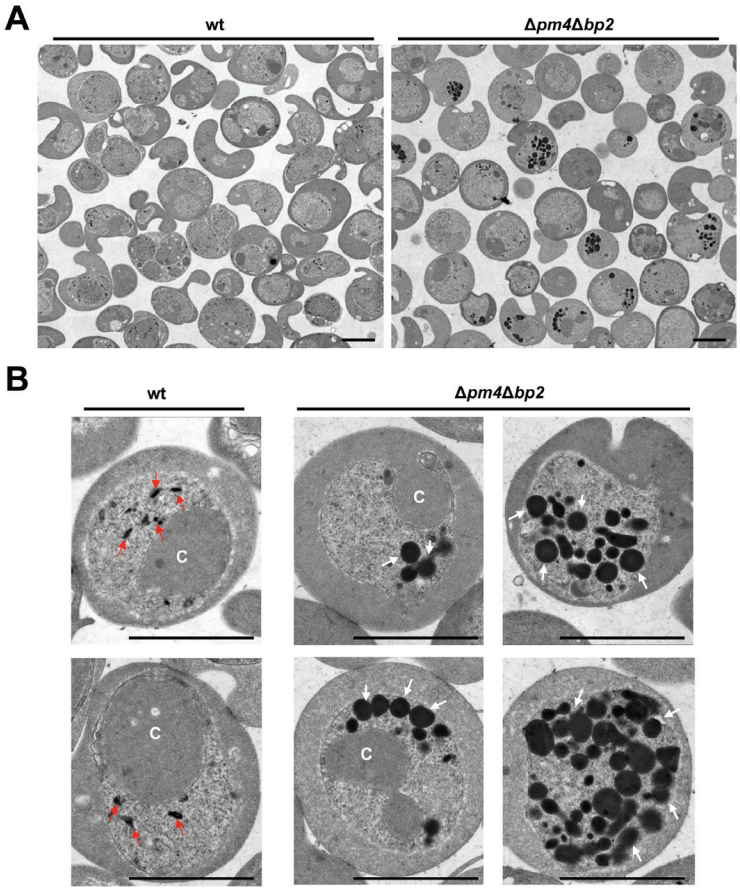

Figure S6. Ultrastructural analysis of wt- and Δ*pm4*Δ*bp2*-trophozoites

A. Electron micrographs of red blood cells infected with wt- or Δ*pm4*Δ*bp2*-trophozoites showing differences in the number, morphology and electron-dense staining of intracellular vesicles within their cytoplasm. Scale bars, 5 µm.

B. Hz crystals (red arrow heads) and cytostomes (C) in both wt- and Δ*pm4*Δ*bp2*-trophozoites. The presence and accumulation of dark-staining vesicles (DSV, white arrow heads) is only visible in Δ*pm4*Δ*bp2*-trophozoites. Scale bars, 5 µm.

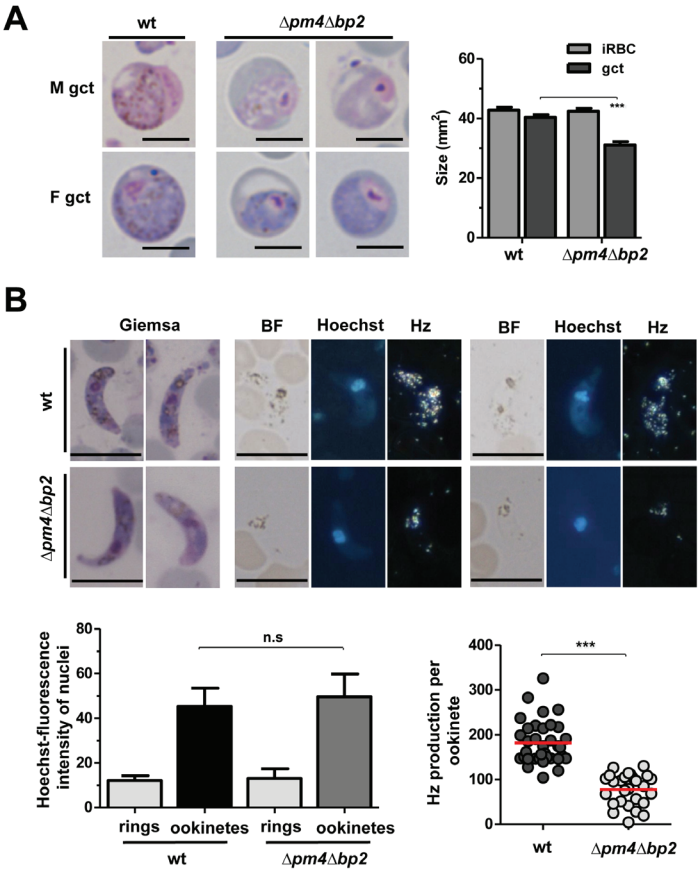

Figure S7. Gametocytes of Δ*pm4*Δ*bp2* are fertile despite their smaller size and reduced hemozoin production

A. Δ*pm4*Δ*bp2*-parasites produce gametocytes with a smaller size compared to wt-gametocytes. Mature wt male (M) and female (F) gametocytes (gct) usually occupy the entire volume of the iRBC and are characterized by abundant Hz crystals scattered throughout the cytoplasm, a single excentric located nucleus that is enlarged in male gametocytes, dark blue stained cytoplasm in females and pink stained cytoplasm in males. Uninuclear parasites with characteristics of mature male and female gametocytes (excentric nucleus, blue or pink stained cytoplasm) were readily detected on Giemsa-stained smears of tail blood obtained from mice infected with Δ*pm4*Δ*bp2*-parasites (left panel). Size measurements of gametocytes in Giemsa-stained smears showed a significant reduction in size of the Δ*pm4*Δ*bp2* gametocytes (right panel). Scale bars, 5 µm.

B. Female Δ*pm4*Δ*bp2* gametes are fertilized and develop into ookinetes with the same characteristics as wt-ookinetes, including a banana shaped morphology and a centrally located, enlarged nucleus. However, the Δ*pm4*Δ*bp2*-ookinetes show strongly reduced or absent Hz clusters. BF, bright-field.

C. Normal DNA content and reduced Hz levels in Δ*pm4*Δ*bp2*-ookinetes.

Nuclear DNA content of Δ*pm4*Δ*bp2*- and wt-ookinetes as determined by Hoechst-fluorescence intensity measurements. The mean fluorescence intensity of haploid ring-form nuclei (white arrows) of Δ*pm4*Δ*bp2* and wt are 13.0 and 12.1 RLI (relative light intensity), respectively. The Δ*pm4*Δ*bp2* and wt ookinetes show similar (tetraploid) DNA content and both have similarly enlarged nuclei, with RLI values of 49.6 and 45.3, respectively (n.s, student T-test, not significant, n>25). The amount of Hz in individual ookinetes (n>25) is determined by

measuring relative light intensity (RLI) of polarized light. The Hz level in Δ*pm4*Δ*bp2* parasites ookinetes is significantly lower (57% less) than wt ookinets (*** P<0.0001, student T-test).

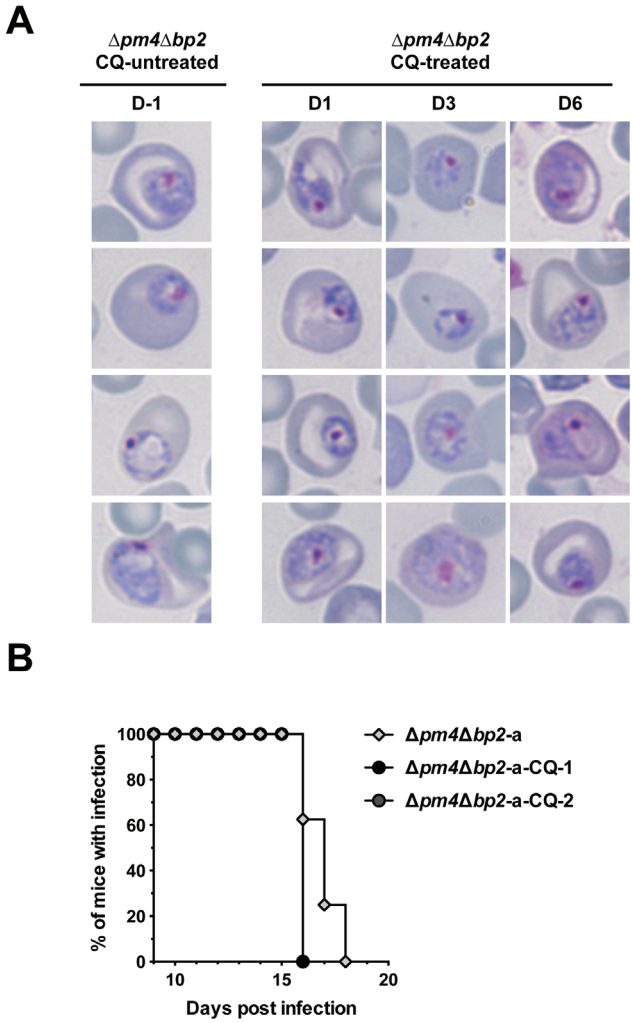

Figure S8. Cloroquine treatment of Δ*pm4*Δ*bp2*-infected BALB/c mice

A. Trophozoites of Δ*pm4*Δ*bp2*-parasites before chloroquine (CQ) treatment and at different days after start of CQ treatment. Untreated Δ*pm4*Δ*bp2*-parasites 1 day before CQ treatment (D-1) show an identical morphology to Δ*pm4*Δ*bp2*-parasites at day 1, 3 and 8 (D1, D3, D6) during CQ treatment with respect to size, absence of Hz pigment granules, accumulation of intracellular vacuoles and amoeboid morphology (see Figure S5).

B. Clearance of Δ*pm4*Δ*bp2*-parasites in infected mice that were treated (CQ-1,2) or non-treated (NT) with CQ. In 2 experiments, Δ*pm4*Δ*bp2*-parasites were cleared in all mice (n=10) to undetectable levels (as examined by microscopy) on day 16 post-infection in CQ-treated mice (7 days after CQ treatment). In non-treated mice (n=8), parasites were cleared between 16-18 days post-infection.

Table S1. Gene deletion experiments to disrupt the *P. berghei* genes encoding hemoglobinases

Gene deletion mutant	Gene name	Gene ID	DNA construct name	Experiment No., Mutant name[1]	Parent line[2]	RMgmDB ID[3]
Unsussessful attempts						
-	bergelysin (bln)	PBANKA_113700	PCR1541	1502	676m1cl1	RMgm-804
			pL1557	1543	676m1cl1	
			pLTgLysin	lysinko 1-2-3	676m1cl1	
-	M1- family alanyl Aminopeptidase (aap)	PBANKA_141030	PCR1877	2058, 2087, 2111	1037m1f1cl1, 820cl1m1cl1	RMgm-806
			pLTgAPN	aapko 1-2-3	676m1cl1	
-	Heme detoxification protein (hdp)	PBANKA_131060	PCR1690	1748, 1778, 2212	676m1cl1	RMgm-807
			PCR1762	2208, 2213	cl15 cycI, 676m1cl1	
			pPhHDP	hdpko 1-2-3	cl15cy1	
Mutants						
Δ*pm4*	plasmepsin 4	PBANKA_103440	PCR1597	1688cl1	1037m1f1cl1	RMgm-808
Δ*bp2*-a	berghepain-2	PBANKA_093240	pLTgPain2	Pain2cl8	1037m1f1cl1	
Δ*bp2*-b			pL1602	1619cl1	1037m1f1cl1	RMgm-809
Δ*dpap1*-a	dipeptidyl aminopeptidase 1	PBANKA_093130	pLDPA	DPAkocl5	1037m1f1cl1	
Δ*dpap1*-b			PCR1833	1962cl1	cl15cy1	RMgm-810
Δ*dpap2*	dipeptidyl aminopeptidase 2	PBANKA_146070	PCR1875	2056cl1	1037m1f1cl1	RMgm-811
Δ*dpap3*-a	dipeptidyl aminopeptidase 3	PBANKA_100240	PCR1876	2057cl1	1037m1f1cl1	RMgm-812
Δ*dpap3*-b				2110cl1	1037m1f1cl1	
Δ*app*-a	aminopeptidase P	PBANKA_131810	PCR1924	2129cl2	1037m1f1cl1	RMgm-813
Δ*app*-b				2248cl1	1037m1f1cl1	
Δ*lap*	M17-family leucyl aminopeptidase	PBANKA_130990	PCR1878	2112cl3	1037m1f1cl1	RMgm-814
Δ*dap*	M18-family aspartyl aminopeptidase	PBANKA_083310	PCR1879	2060cl1	1037m1f1cl1	RMgm-815
Δ*bp1*	berghepain-1	PBANKA_132170	pL1976_3	2250cl1	1037m1f1cl1	RMgm-816
Δ*pm4*Δ*bp2*-a	plasmepsin 4	PBANKA_103440	PCR1597	1863cl1	Δ*bp2*-b^{-sm}	RMgm-817
Δ*pm4*Δ*bp2*-b	berghepain-2	PBANKA_093240		1864cl1	Δ*bp2*-b^{-sm}	

[1] Experiment number for independent transfection experiments: the unsuccessful attempts (3 times) and the experiment number/clone of the gene deletion mutants
[2] Parent *P. berghei* ANKA line in which the genes were targetted for deletion
[3] The ID number of the mutants (or of the unsuccessful attempts for gene deletion) in the RMgm database (www.pberghei.eu)

Table S2. Targeting constructs and primers

Gene	DNA Construct	Basic construct	Descrip-tion	No.	Primer sequences *	Restriction sites	localzation
plasmepsin 4	pL1873	pL0048	P1	L6861	GAACTCGTACTCCTTGGTGACGTCGCGACCTTGTCGGGGTACTCAG	*Nru*I	*pm4* 5'-targeting sequence, F
(pm4)			P2	L6862	CATCTACAAGCATCGTCGACCTCAAGCTTCCCAATCTCTTTAATAAGG		*pm4* 5'-targeting sequence, R
			P3	L6863	CCTTCAATTTCGGATCCACTAGACACGTACCATAACATGC		*pm4* 3'-targeting sequence, F
			P4	L6864	AGGTTGGTCATTGACACTCAGCTCGCGATTCCTACAAATCAAATATCACG	*Nru*I	*pm4* 3'-targeting sequence, R
bergheipain 2	pLTgPain2-a	pLTgDHFR	P1	RS443	CCGGGCCCGCGGGGTTTCTATCTATATTTATTTCTGC	*Apa*I	*bp2* 5'-targeting sequence, F
(bp2)			P2	RS444	CCATCGATTTATGTTTCTATGTTAATTTTTTTTTGC	*Cla*I	*bp2* 5'-targeting sequence, R
			P3	RS445	GGAATTCAAATAATATTATGTACCGATAGG	*EcoR*I	*bp2* 3'-targeting sequence, F
			P4	RS446	CGGGATCCTGGAATCGCCCTTTTATAATGC	*BamH*I	*bp2* 3'-targeting sequence, R
	pL1602	pL0035	P1	L5458	GAACTCGTACTCCTTGGTGACGAAGCTTTATTATATGCGTATACCCTGC	*Hind*III	*bp2* 5'-targeting sequence, F
			P2	L5459	CAGATCTATCGATCCGCGGCCGCGGAACATACAATTTAGTGCATGG	*Ksp*I	*bp2* 5'-targeting sequence, R
			P3	L5460	CGATATCTGATCACCCGGGGGTACCATAGTTGCACTTTATGGACG	*Asp718*I	*bp2* 3'-targeting sequence, F
			P4	L5461	AGGTTGGTCATTGACACTCAGCGAATTCGAAGGATTAACTGCTACAGAC	*EcoR*I	*bp2* 3'-targeting sequence, R
berghelysin	PCR1541	pL0048	P1	L5101	GAACTCGTACTCCTTGGTGACGGGTACCCATTAATATGCTAAGCATTACAC	*Asp718*I	*bln5'*-targeting sequence, F
(bln)			P2	L5102	CATCTACAAGCATCGTCGACCTCTCTTCACATAATTCACTTGAC		*bln5'*-targeting sequence, R
			P3	L5103	CCTTCAATTTCGGATCCACTAGACAATTGATAGACCTAGAAGAG		*bln3'*-targeting sequence, F
			P4	L5104	AGGTTGGTCATTGACACTCAGCAGTACTGTTGCATACAATGAGATACTC	*Sca*I	*bln3'*-targeting sequence, R
	pL1557	pL0035	P1	L5109	CCCAAGCTTCATTAATATGCTAAGCATTACAC	*Hind*III	*bln5'*-targeting sequence, F
			P2	L5110	TCCCCGCGGTCTTCACATAATTCACTTGAC	*Ap*I	*bln5'*-targeting sequence, R
			P3	L5111	CGGGGTACCACAATTGATAGACCTAGAAGAG	*Asp718*I	*bln3'*-targeting sequence, F
			P4	L5112	CCGCTCGAGGTTGCATACAATGAGATACTC	*Xho*I	*bln3'*-targeting sequence, R
	pLTgLysin	pLTgDHFR	P1	RS447	CCGGGCCCGCGGAAATATAGTTCCAACTTTAATTTAAAGG	*Apa*I	*bln5'*-targeting sequence, F
			P2	RS448	CCATCGATTTATTATACTGCACATATATAAAAAAATGC	*Cla*I	*bln5'*-targeting sequence, R
			P3	RS449	GGAATTCGTTTTTGTTCACTCCTTTTTTACATATAAAC	*EcoR*I	*bln3'*-targeting sequence, F
			P4	RS450	CGGGATCCACAATGAGATACTCTTCATAAAAATTTG	*BamH*I	*bln3'*-targeting sequence, R
dipeptidyl peptidase 1	pLTgdpap1a	pLTgDHFR	P1	RS578	CCGGGCCCGCGGGCATGTAATGCGTATATTCG	*Apa*I	*dpap1* 5'-targeting sequence, F
(dpap1)			P2	RS579	CCATCGATCGAATTTTGGGGTTAATTATATCC	*Cla*I	*dpap1* 5'-targeting sequence, R
			P3	RS580	GGGGTACCGAGTATATGCTTTCATGGAAATG	*Kpn*I	*dpap1* 3'-targeting sequence, F
			P4	RS581	CGGGATCCTCATAATTCATTAAAAGTGATATTAAAG	*BamH*I	*dpap1* 3'-targeting sequence, R

	PCR1833	pL0048	P1	L6855	GAACTCGTACTCCTTGGTGACGTCGCGAGCATGTAATGCGTATATTCG	*Nru*I	*dpap1* 5′-targeting sequence, F
			P2	L6856	CATCTACAAGCATCGTCGACCTCGAATTTTGGGGTTAATTATATCC		*dpap1* 5′-targeting sequence, R
			P3	L6857	CCTTCAATTTCGGATCCACTAGTATATGCTTTCATGGAAATGTG		*dpap1* 3′-targeting sequence, F
			P4	L6858	AGGTTGGTCATTGACACTCAGCTCGCGATAATTCATTAAAAGTGATATTAAAGAG	*Nru*I	*dpap1* 3′-targeting sequence, R
dipeptidyl peptidase 2 (dpap2)	PCR1875	pL0048	P1	L6925	GAACTCGTACTCCTTGGTGACGTCGCGATTTTTGTGGGTACAATGTG	*Nru*I	*dpap2* 5′-targeting sequence, F
			P2	L6926	CATCTACAAGCATCGTCGACCTCATAAATATAATGCCACTGCTC		*dpap2* 5′-targeting sequence, R
			P3	L6927	CCTTCAATTTCGGATCCACTAGGTATTTGCGCCCTTTTTC		*dpap2* 3′-targeting sequence, F
			P4	L6928	AGGTTGGTCATTGACACTCAGCTCGCGAATTAAAATGTGCTATATGCAG	*Nru*I	*dpap2* 3′-targeting sequence, R
dipeptidyl peptidase 3 (dpap3)	PCR1876	pL0048	P1	L6931	GAACTCGTACTCCTTGGTGACGTCGCGATTCATTTTAGGCGGAGTG	*Nru*I	*dpap3* 5′-targeting sequence, F
			P2	L6932	CATCTACAAGCATCGTCGACCTCTGAAAACGGATAACTATATGTG		*dpap3* 5′-targeting sequence, R
			P3	L6933	CCTTCAATTTCGGATCCACTAGTATAATGGGCCTGTAGCTG		*dpap3* 3′-targeting sequence, F
			P4	L6934	AGGTTGGTCATTGACACTCAGCTCGCGATAATGCCAATTTTTTTTAATGAG	*Nru*I	*dpap3* 3′-targeting sequence, R
Aminopeptidase P (app)	PCR1924	pL0048	P1	7103	GAACTCGTACTCCTTGGTGACGTCGCGATATTACACATAAGGGCTGAATTG	*Nru*I	*app*5′-targeting sequence, F
			P2	7104	CATCTACAAGCATCGTCGACCTCATATGGGCATATATTATATACATATAC		*app*5′-targeting sequence, R
			P3	7105	CCTTCAATTTCGGATCCACTAGCCATTTATTATATGTGTGTTTTAATTC		*app*3′-targeting sequence, F
			P4	7106	AGGTTGGTCATTGACACTCAGCTCGCGAAACGGTAAAATTATCAAACAAAG	*Nru*I	*app*3′-targeting sequence, R
	pLTgAPP	pLTgDHFR	P1	RS695	GGGGGGGCCCGCGGGGCAATATCATAATTATTATATCTTC	*Apa*I	*app*5′-targeting sequence, F
			P2	RS696	GGGGATCGATGTTTGCATATATAAGCGAATTTATACC	*Cla*I	*app*5′-targeting sequence, R
			P3	RS697	GGGGGAATTCTAGAATTTTGTATATATGTATTTAGTTGA	*EcoR*I	*app*3′-targeting sequence, F
			P4	RS698	AAGGAAAAAAGCGGCCGCCAAAACTAGACAAAGAAGAAACC	*Not*I	*app*3′-targeting sequence, R
M1- family alanyl Aminopeptidase (aap)	PCR1877	pL0048	P1	L6945	GAACTCGTACTCCTTGGTGACGTCGCGAATAATAGTATAAAGGGAATTATATGC	*Nru*I	*aap* 5′-targeting sequence, F
			P2	L6946	CATCTACAAGCATCGTCGACCTCACATAAATATATACATGTGTATTTGC		*aap* 5′-targeting sequence, R
			P3	L6947	CCTTCAATTTCGGATCCACTAGTAATATATGTATTTCCCACTTTGC		*aap* 3′-targeting sequence, F
			P4	L6948	AGGTTGGTCATTGACACTCAGCTCGCGATATATTTATGGGTTTGTTTTTCC	*Nru*I	*aap* 3′-targeting sequence, R
	pLTgAPN	pLTgDHFR	P1	RS715	GGGGGGGCCCGCGGCTTATTGTATCCCTTGGCATTTG	*Apa*I	*aap*5′-targeting sequence, F
			P2	RS716	GGGGATCGATATCGTATAGTATTATTTATCATGCAAG	*Cla*I	*aap*5′-targeting sequence, R
			P3	RS717	GGGGGAATTCACAAATAAAATGTGAAAGTAAAGTTTTAC	*EcoR*I	*aap*3′-targeting sequence, F
			P4	RS718	AAGGAAAAAAGCGGCCGCTGTGAGACTTTCCATATAAGGAATAC	*Not*I	*aap*3′-targeting sequence, R
M17-family leucyl aminopeptidase (lap)	PCR1878	pL0048	P1	L6963	GAACTCGTACTCCTTGGTGACGTCGCGAGGATTAAGAGATGATCGTAGTG	*Nru*I	*lap* 5′-targeting sequence, F
			P2	L6964	CATCTACAAGCATCGTCGACCTCTATTATGCACAAATTGAAAATACG		*lap* 5′-targeting sequence, R

			P3	L6965	CCTTCAATTTCGGATCCACTAGCAAAGTGGTAGTTTTTGTTATATC		*lap* 3'-targeting sequence, F
			P4	L6966	AGGTTGGTCATTGACACTCAGCTCGCGATACACAACAATGAAAAAAAAACTG	*Nru*I	*lap* 3'-targeting sequence, R
M18-family aspartyl aminopeptidase (dap)	PCR1879	pL0048	P1	L6971	GAACTCGTACTCCTTGGTGACGTCGCGATGTTGAAGGCATAATAAAACAG	*Nru*I	*dap* 5'-targeting sequence, F
			P2	L6972	CATCTACAAGCATCGTCGACCTCATATACATACGATATGCCTACAC		*dap* 5'-targeting sequence, R
			P3	L6973	CCTTCAATTTCGGATCCACTAGCAGTCAAATTATAAGTACAAAGG		*dap* 3'-targeting sequence, F
			P4	L6974	AGGTTGGTCATTGACACTCAGCTCGCGACATTAAAATGCATATTGCATGG	*Nru*I	*dap* 3'-targeting sequence, R
	pLTgDAP	pLTgDHFR	P1	RS761	GGGGGCCCGCGGCGATTTTATTTACTCTTGTTTTTTTATG	*Apa*I	dpa 5'-targeting sequence, F
			P2	RS762	GGGGATCGATCAAACGTTGATAAATGTATAAAAATAATG	*Cla*I	*dpa* 5'-targeting sequence, R
			P3	RS763	GGGGGAATTCGGTACCGAGTATATGCTTTCATGGAAATG	*EcoR*I	dpa 3'-targeting sequence, F
			P4	RS764	AAGGAAAAAAAGCGGCCGCTGGATCCTCATTAAAAGTGATATTAAAGAGTATAC	*Not*I	*dpa* 3'-targeting sequence, R
Heme detoxification protein (hdp)	PCR1690	pL0040	P1	L5868	GAACTCGTACTCCTTGGTGACGGGTACCAATTGGTGCCATAACCAG	*BamH*I	*hdp* 5'-targeting sequence, F
	PCR1762		P2	L5869	CATCTACAAGCATCGTCGACCTCTCGATCAACCGATTTAGC		*hdp*5'-targeting sequence, R
			P3	L5870	CCTTCAATTTCGGATCCACTAGCACTTGCATGCTATTGTC		*hdp*3'-targeting sequence, F
			P4	L5871	AGGTTGGTCATTGACACTCAGCGGTACCCATGATGCCTTCATATGTG	*BamH*I	*hdp* 3'-targeting sequence, R
	pLhHDP	pLTgDHFR	P1	RS724	CCGGGCCCGCGGCAGCCACTATACTATTTTTATGCTG	*Apa*I	*hdp* 5'-targeting sequence, F
			P2	RS725	GGGGATCGATCGGAAGCATTCACATAAATATTGC	*Cla*I	*hdp* 5'-targeting sequence, R
			P3	RS726	GGGGGAATTCCTATTTAAATGAAGATTTTCCATATATTCAG	*EcoR*I	*hdp* 3'-targeting sequence, F
			P4	RS727	AAGGAAAAAAGCGGCCGCGGTTGAATCCTAATTCAGTATTGATTG	*Not*I	*hdp* 3'-targeting sequence, R
			anchor-tag primers				
				4661	GAACTCGTACTCCTTGGTGACG		anchor-tag primer, F
				4662	AGGTTGGTCATTGACACTCAGC		anchor-tag primer, R

* Red: Restriction sites
Blue: 5'- extensions homologues to the h*dhfr*::*yfcu* selectable marker cassette from pL0048
Green: 5'- extensions homologues to the anchor tag primers 4661/4662

Table S3. Primers for genotyping

Genes	No.	Primer sequences	Description	Integration PCR pair	Product size (bp)
Primers for PCR analyses					
pm4	L5516	TTATGGGGATCCATATTTCAC	*pm4* 5' in-F	L4906	1364
	L5517	CATGCGAATAAATGCTCAG	*pm4* 3' in-R	L1662	1122
	L5518	TCCGAATATTTAACAATTCGTG	*pm4* ORF-F		869
	L5519	ATGAAAGGTACTGGAATACTC	*pm4* ORF-R		
bp2	RS835	TCTACAAGAATAAAAAGTTTCC	*bp2*-a 5' in-F	RS32	879
	RS836	TATTACATCTATATAAGAATCATGC	*bp2*-a 3' in-R	RS110	1075
	RS514	CACCATGAATTACCATTCTAGCCATCATATTAGAC	*bp2*-a ORF-F		1407
	RS515	TTATTCAATTATAGGAGCATAACCTTGTAC	*bp2*-a ORF-R		
	RS516	TTAAGTGAACAACAATTAGTTGATTGTGC	*bp2*-a ORF-F		516
	L5024	ATTGTTTATCGAGGAATTCG	*bp2*-b 5' in-F	L3211	1299
	L5025	TGGATATTCTCACGATTACC	*bp2*-b 3' in-R	L1662	1009
	L5026	GTATGTTTGGTTTTACCGTC	*bp2*-b ORF-F		1108
	L5027	CACATAAACCATCCATGTC	*bp2*-b ORF-R		
bln	L5105	TGTTACATATTTATGGCATTCC	*bln* 5' in-F	L4770	999
	L5106	GCCAACTAGTACAAATATACAC	*bln* 3' in-R	L4771	990
	L5107	GACCCATTAGATGCTGAG	*bln* ORF-F		694
	L5108	GTTCCACAGCATCATCTC	*bln* ORF-R		
dadp1	RS672	CAAACATACAAAAATAAACACC	*dapa1*-a 5'in-F	RS32	875
	RS673	TGTTATAATTCCCTTATATGT	*dapa1*-a 3'in-R	RS110	903
	RS582	CACCGATAATGAACACAGAGAAAATTGGAAC	*dapa1*-a ORF-F		856
	RS583	TTACATTTGAGATGCAATATAACATGAACC	*dapa1*-a ORF-R		
	L6204	GCTTGTTTTATTTCCCTTTATTTTAC	*dapa1*-b 5' in-F	L4770	875
	L6205	GAGTAATGTTATAATTCCCTTATATGTG	*dapa1*-b 3' in-R	L4771	903
	L6206	GTTGTTTTTATGCTGAAAAATACG	*dapa1*-b ORF-F		856
	L6207	AGTACATTTTTTGGCATGTG	*dapa1*-b ORF-R		
dadp2	L6935	ATTCTCAACAAATGGGCAACTG	*dapa2* 5' in-F	L4770	853
	L6936	TCTTTAAACTCGACATTTTTTCC	*dapa2* 3' in-R	L4771	951
	L6937	CTCCCTATTCATGCTCTTATGG	*dapa2* ORF-F		922
	L6938	CTACAATACTTGGACATTCCTC	*dapa2*ORF-R		
dadp3	L6941	CAATGCAAGTAGCAGAGAATG	*dpap3* 5' in-F	L4770	893
	L6942	CTTCATTACGAGATTAAAAATTCAC	*dpap3* 3' in-R	L4771	819
	L6943	ATCCCTGTTCATTGCTTGAG	*dpap3* ORF-F		1181
	L6944	AGTATCTGCATTAACATCTAGAG	*dpap3* ORF-R		
app	L7107	AAGTATTATAAAATTAGCGCAAACAG	*app* 5' in-F	L4770	1003
	L7108	TCATTTTGCTTTATTTTCTCTTTTG	*app* 3' in-R	L4771	1009
	L7109	ATGCGTATAAATTCGCTTATATATG	*app* ORF-F		996
	L7110	CAAAGAATCTACATCAGGGTTCTC	*app* ORF-R		
aap	L6949	TGTGAATTTGCGGAGATGTTG	*aap* 5' in-F	L4770	928
	L6950	AATTATTAGTAAAAATGCGAAAGG	*app* 3' in-R	L4771	1068
	L6951	AGAACAGATTACAAACCAAGTG	*aap* ORF-F		912
	L6952	ACCAGTATAGTTATGGAAATATTCG	*aap* ORF-R		
lap	L6967	AAGTAATGCTTTTACCCTTTCTG	*lap* 5' in-F	L4770	1051
	L6968	ATATATACTCCCTTATACCACGTC	*lap* 3' in-R	L4771	1088

	L6969	AAAACAATTACAATAGTGATTGTC	*lap* ORF-F		988
	L6970	GGATACATACTACCTTTTCCTACTG	*lap* ORF-R		
dap	L6975	TATGGGTGTCCTAATTTTAACTG	*dap* 5' in-F	L4770	880
	L6976	AGTTAATCGAAAGCACTGATAC	*dap* 3' in-R	L4771	893
	L6977	GATAAAAAGGCACGAGAATATG	*dap* ORF-F		1037
	L6978	AAACTTCCATATATTTCATCTACTG	*dap* ORF-R		
Universal primers					
	L695	AATATTCATAACACACTTTTAAGC	5'*pbdhfr*/*ts* R		
	L3211	GCACACAACATACACATTTTTACAG	3'*pbdhfr*/*ts* R		
	L4906	CGACTAGTTAATAAAGGGCAC	5'*pbeef1a* R		
	L1662	GATTCATAAATAGTTGGACTTG	3'*pbdhfr*/*ts* F		
	L4770	CATCTACAAGCATCGTCGACCTC	anchor-tag R		
	L4771	CCTTCAATTTCGGATCCACTAG	anchor-tag F		
	L4598	GGACAGATTGAACATCGTCG	*tgdhfr*/*ts* F		1059
	L4599	GTGTAGTCTGTGTGCATGTC	*tgdhfr*/*ts* R		
	RS1900	CGGGATCCATGCATAAACCGGTGTGTC	*tgdhfr*/*ts* F		1850
	RS1901	CGGGATCCAAGCTTCTGTATTTCCGC	*tgdhfr*/*ts* R		
	L4698	GTTCGCTAAACTGCATCGTC	h*dhfr* F		787
	L4699	GTTTGAGGTAGCAAGTAGACG	y*fcu* R		
Primers for PCR probes and RT-PCR					
	L692	CGCGGATCCATGCATAAACCGGTGTGTC	3'*pbdhfr*/*ts* F		404
	L693	CGCGGATCCGCTAGACAGCCATCTCCAT	3'*pbdhfr*/*ts* R		
	L886	GGAAGATCTATGGTTGGTTCGCTAAACTGCATCG	h*dhfr* F		582
	L887	GGAAGATCTTTAATCATTCTTCTCATATACTTC	h*dhfr* R		
	L644	GGAAACAGTCCATCTATAATTG	lsu rrna (A-type)		
	RS32	CAAACATACAAAAATAAACACC	5'*pbdhfr*/*ts* R		
	RS110	CTTTATGTCCACAACATCATC	3'*pbdhfr*/*ts* F		
	RS782	TGGAGCAGGAAATAACTGGG	*pbTub*F		402
	RS783	ACCTGACATAGCGGCTGAAA	*pbTub*R		
	7422	AACATTACCACAAGCAGTATCG	*bp1* ORF-F		1001
	7423	CCATCACATCCAAAATTGTCAC	*bp1*ORF-R		

pb = *P. berghei*, *tg* = *T. gondii;* h = human, y = yeast

5' in = 5' integration PCR; 3' in = 3' integration PCR